

AIAA Aerospace Sciences Meeting and Exhibit, 7-10 January 2008, Reno, NV

Comparative Study of 3D Wing Drag Minimization by Different Optimization Techniques

Boris Epstein*

Academic College of Tel-Aviv, Israel

Antony Jameson†

Stanford University, USA

Sergey Peigin‡

Israel Aerospace Industries, Israel

Dino Roman§

The Boeing Company, USA

Neal Harrison¶

The Boeing Company, USA

John Vassberg||

The Boeing Company, USA

The main goal of this paper is to document a comparative study of different CFD based optimization techniques applied to the solution of a 3D wing drag minimization problem. To achieve this objective, three optimization tools were used: SYN107 (Intelligent Aerodynamics Int'l), MDOPT (The Boeing Company) and OPTIMAS (Israel Aerospace Industries). The first tool employs gradient-based search techniques using the "continuous" adjoint equation, the second one is a response-surface method, while the last one uses a floating-point Genetic Algorithm as its search engine. As the starting geometry, the public domain DPW-W1 wing (a test-case for the 3rd Drag Prediction Workshop) was used. The comparisons included herein are provided in three stages: verification of solutions of the initial geometry by the CFD tools employed in the optimizations, optimization of the initial geometry to minimum drag, and cross-analysis of optimal shapes achieved by the optimization tools using all CFD tools employed. The cross-analysis also includes results from an independent CFD method which was not used in any of the optimization efforts. These results help quantify the level of variation that is inherent in and can be expected from application of the current state-of-the-art aerodynamic optimization methods.

The present work may be regarded as a move towards the construction of reliable test-cases for an aerodynamic shape optimization problem. Another goal of this collaborative investigation is to collect lessons learned from this pilot project to help develop a model for an Aerodynamic Optimization Workshop.

*Professor, Computer Sciences Department, Member AIAA

†Thomas V. Jones Professor of Engineering, Fellow AIAA

‡Professor, Aerodynamic Department, Senior Member AIAA

§Associate Technical Fellow, Associate Fellow AIAA

¶Aerodynamics Engineer, Member AIAA

||Boeing Technical Fellow, Associate Fellow AIAA

I. Introduction

In the development of commercial aircraft, aerodynamic design plays a leading role during the preliminary design stage where the external aerodynamic shape is typically finalized. This phase is estimated to cost 60-120 million dollars Ref. [1]. The final design would be normally carried out only upon the commercially promising completion of the preliminary stage. Hence, the preliminary design stage is crucial for the overall success of the project.

To additionally underline the importance of drag minimization, consider the task of delivering a payload between distant destinations. Based on the Breguet range equation, which applies to long-range missions of jet-aircraft, the operator would have to reduce the pay-load (and thus the revenue) by 7.6% to recover a 1.0% increase in drag (see Ref. [1]). Since most airlines operate on small margins, this would most likely no longer be a profit-generating venture. This example illustrates that a 1% delta in total drag is a significant change.

That is why CFD driven aerodynamic shape design has aroused steadily increasing interest Ref. [2-9]. Along with improvement in the accuracy of CFD, its contribution to aerodynamic design steadily grows. In fact, the past three decades have brought a revolution in the entire process of aerodynamic design due to the increasing role of computational simulation.

Early on, the applicability of CFD to aerodynamic design was confined to flow analysis in a limited range of flight conditions and aerodynamic shapes. Additional limitations were due to the variable levels of accuracy in the prediction of different aerodynamic characteristics. For example, accurate CFD estimation of sensitive flow characteristics such as drag and pitching moment of three-dimensional wings became available only in recent years when Navier-Stokes methods reached an acceptable level of maturity, while reasonably accurate estimates of $\partial C_L / \partial \alpha$ were attainable in the middle of the 1970's using linear panel methods.

At the present time, the maturity of CFD solvers for accurate drag estimation and the efficiency level of search engines enables an attempt at the aerodynamic optimization problem in an engineering environment. With this end in view, CFD based aerodynamic optimizers must be verified by means of reliable test-cases. This verification presents a complicated problem since it is impractical to test every optimal shape in a wind tunnel.

In this connection, the main goal of this paper is to perform a comparative study of several different CFD based optimization techniques applied to the solution of a 3D wing drag minimization problem. Specifically, three optimization tools: **SYN107** (Intelligent Aerodynamics), **MDOPT** (The Boeing Company) and **OPTIMAS** (Israel Aerospace Industries) were used. Additionally, the authors desired to better understand the pros & cons of three very different approaches to aerodynamic shape optimization.

This paper presents the first (to the best of the authors' knowledge) attempt to systematically cross-analyze optimizations performed by different optimization tools in all three stages of the optimization process: CFD cross-analysis of the initial geometry (performed by the CFD tools employed in optimization), multiple optimization by three different optimizers, and, finally, CFD cross-analysis of the independently-generated optimal shapes. The cross-analysis phase included application of the three CFD solvers employed in the optimizations, as well as one solver which was not utilized during any of the optimization efforts.

The present work may be regarded as a move towards the construction of reliable test-cases for the aerodynamic shape optimization problem. Further, this pilot project has collected lessons learned and may serve as a model for an Aerodynamic Optimization Workshop.

II. Statement of the Problem

The input parameters of the aerodynamic configuration design are the aerodynamic performance requirements. These include the prescribed cruise lift, Mach number, altitude and maximum allowable drag values in order to ensure that the aerodynamic goals of the aircraft design (such as range, payload, fuel volume, etc.) are achieved. The desired geometry is sought in the class of solutions which satisfy different geometrical, aerodynamic and multidisciplinary constraints. Specifically, constraints are usually placed upon airfoils' thickness, pitching moment, minimum C_L^{max} at the take-off condition, etc.

The design goal is to develop a geometry with as low a drag as possible at cruise conditions, which at the same time satisfies the above constraints. Based on the above ideas, the mathematical formulation of the optimization problem may be expressed as follows.

The objective of the general multipoint optimization problem is to minimize the weighted combination C_D^{wtd} of drag coefficients at the main design and secondary design points (flight conditions)

$$C_D^{wtd} = \sum_{k=1}^K w_k C_D(k),$$

where K is the total number of the design points.

The solution is sought in the class of wing shapes subject to the following classes of constraints:

1) Aerodynamic constraints such as prescribed constant total lift coefficient $C_L^*(k)$ and minimum allowed pitching moment $C_M^*(k)$:

$$C_L(k) = C_L^*(k), \quad C_M(k) \geq C_M^*(k) \quad (1)$$

2) Geometric constraints on the shape of the wing surface in terms of properties of sectional airfoils at the prescribed wing span locations: relative thickness $(t/c)_i$, relative local thickness $(\Delta y/c)_{ij}$ at the given chord locations $(x/c)_{ij}$ (beam constraints), relative radius of leading edge $(R/c)_i$, trailing edge angle θ_i :

$$(t/c)_i \geq (t/c)_i^*, \quad (\Delta y/c)_{ij} \geq (\Delta y/c)_{ij}^*, \quad (R/c)_i \geq (R/c)_i^*, \quad \theta_i \geq \theta_i^* \quad (2)$$

$$i = 1, \dots, N_{ws}, \quad j = 1, \dots, N_{bc}(i)$$

where N_{ws} is the total number of sectional airfoils subject to optimization, $N_{bc}(i)$ is the total number of beam constraints at section i , and values $(t/c)_i^*$, $(\Delta y/c)_{ij}^*$, θ_i^* , $(R/c)_i^*$, C_L^* and C_M^* are prescribed parameters of the problem.

III. Test-Case Description

1. Initial geometry. The public domain DPW-W1 wing was used as the initial geometry for the aerodynamic optimizations. Reference quantities for this wing are: $S_{ref} = 290,322 \text{ mm}^2$, $C_{ref} = 197.556 \text{ mm}$, $X_{ref} = 154.245 \text{ mm}$ (relative to the wing root leading edge), and a semispan value of $b/2 = 762 \text{ mm}$. During the optimizations, the wing planform was fixed.

2. Design points.

2.1. $M = 0.76$, $C_L = 0.5$, $Re = 5 \cdot 10^6$ (main design point)

2.2. $M = 0.78$, $C_L = 0.5$, $Re = 5 \cdot 10^6$ (high Mach secondary design point)

2.3. $M = 0.20$, $C_L^{max}(\text{optimal}) \geq C_L^{max}(\text{original})$, (take-off secondary design point)

3. Geometrical constraints (per wing design section).

3.1. $(t/c)_i \geq (t/c)_i^*$,

where $(t/c)_i^*$ is the maximum thickness for the original wing defining sections; for $i = 1$ (root), 2 (crank), 3 (tip);

$$(t/c)_1^* = (t/c)_2^* = (t/c)_3^* = 13.5\%$$

3.2. $(t/c)_{ij}(x/c)_{ij} \geq (t/c)_{ij}^*(x/c)_{ij}$,

where $(t/c)_{ij}^*(x/c)_{ij}$ is thickness value of the original wing section at fixed (x/c) locations - representing beam constraints;

$$(x/c)_{11} = (x/c)_{21} = (x/c)_{31} = 0.20, \quad (t/c)_{11}^* = (t/c)_{21}^* = (t/c)_{31}^* = 12.0\%$$

$$(x/c)_{12} = (x/c)_{22} = (x/c)_{32} = 0.75, \quad (t/c)_{12}^* = (t/c)_{22}^* = (t/c)_{32}^* = 5.9\%$$

4. Aerodynamic constraints and penalties.

4.1. $C_M \geq C_M^*$ (C_M^* is equal to the pitching moment value of the original geometry).

4.2. $C_M \geq -\infty$ (unconstrained pitching moment value)

4.3. Pseudo Trim-Drag Penalty: It is assumed that if the value of C_M corresponding to the optimal geometry is not satisfied to condition 4.1, the penalty will be equal to 1 aerodynamic drag count per 0.01 in ΔC_M .

IV. Optimization Tools

Three different optimization tools were used to solve the drag minimization problem: **SYN107** (Intelligent Aerodynamics), **MDOPT** (The Boeing Company) and **OPTIMAS** (Israel Aerospace Industries). The first tool employs gradient-based search techniques using the "continuous" adjoint equation, the second one is a response-surface method, while the last one uses a floating-point Genetic Algorithm as its search engine.

Brief descriptions of these optimization methods are presented below.

A. Optimization Tool SYN107

The optimization tool **SYN107** employs a gradient-based search method. In the gradient calculation, a cost effective technique is used in which the gradient is computed through the solution of an adjoint problem such as that developed in Ref.[10]. The essential idea may be summarized as follows. For flow about an arbitrary body, the aerodynamic properties that define the cost function I are functions of flowfield variables (w) and the physical shape of the body, which may be represented by the function F . Then

$$I = I(w, F)$$

and a change in F results in a change of the cost function

$$\delta I = \frac{\partial I^T}{\partial w} \delta w + \frac{\partial I^T}{\partial F} \delta F$$

Using a technique drawn from control theory, the governing equations of the flowfield are introduced as a constraint in such a way that the final expression for the gradient does not require reevaluation of the flowfield. In order to achieve this, δw must be eliminated from the above equation. Suppose that the governing equation R , which expresses the dependence of w and F within the flowfield domain D , can be written as

$$R(w, F) = 0 \tag{3}$$

Then δw is determined from the equation

$$\delta R = \frac{\partial R}{\partial w} \delta w + \frac{\partial R}{\partial F} \delta F = 0$$

Next, introducing a Lagrange multiplier Ψ with some rearrangement and choosing Ψ to satisfy the adjoint equation

$$\left[\frac{\partial R}{\partial w} \right]^T = \frac{\partial I^T}{\partial w} \quad (4)$$

the term multiplying δw can be eliminated in the variation of the cost function, and we find that

$$\delta I = G \delta F$$

where

$$G = \frac{\partial I^T}{\partial F} - \Psi^T \left[\frac{\partial R}{\partial F} \right]$$

The advantage is that the variation in cost function is independent of δw , with the result that the gradient of I with respect to any number of design variables can be determined without the need for additional flow-field evaluation.

The cost of solving the adjoint equation is comparable to that of solving the flow equation. Hence, the cost of obtaining the gradient is comparable to the cost of two function evaluations, regardless of the dimension of the design space.

Based on this property of the search method, the optimization tool SYN107 automatically sets up the design space by allowing every grid point on the surface to float normal to the surface.

As a gas-dynamic model for evaluation of the cost function the full Navier-Stokes equations are used. Numerical solution of the full Navier-Stokes equations is based on a multigrid multiblock structured code FLO107. This code uses a cell-centered finite volume numerical scheme with the H-CUSP scheme for convective fluxes and central discretization for viscous fluxes, Runge-Kutta local time stepping and implicit residual smoothing.

More details concerning the tool SYN107 may be found in Ref. [11–18],

B. Optimization Tool MDOPT

MDOPT is a Multidisciplinary Design Optimization tool developed at Boeing for air vehicle design and analysis Ref.[19]. The **MDOPT** system contains a collection of technology modules for performing optimization studies by means of a Graphical User Interface (GUI), and combining a set of in-house robust numerical optimization schemes (Design Explorer Ref.[20]) with higher order computational analysis. Global or local direct driven design optimizations may be completed using a variety of multidisciplinary objective and constraint functions including aerodynamics, weight, mission performance, and stability and control characteristics.

The **MDOPT** system is characterized by its scalability to enable the user to frame its application to fit available schedule requirements and computing resources, its flexibility to enable the user to choose from a variety of solvers and other computer aided engineering tools, and its extensibility to enable the system to grow through refinement of existing capabilities and the incorporation of new ones (e.g., the incremental incorporation of additional analysis disciplines or capabilities to address increased geometric complexity).

The illustration in Fig. 1 provides a general outline of the steps required in performing an optimization with MDOPT. Starting at the upper left, the geometry

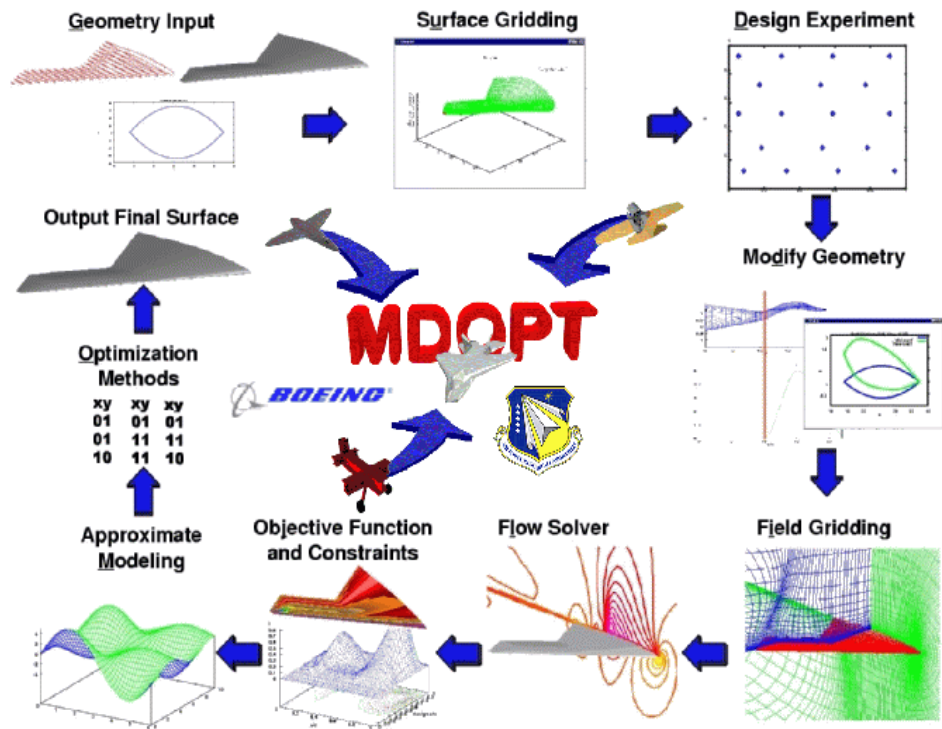


Figure 1. General illustration of MDOPT tool.

is input into the system and surface grids or lofts are created for the input geometry. Next the user defines the design variables and selects a design-of-experiments (DOE). For each design point in the experiment geometry perturbations are created and run through each of the discipline analysis codes. Geometric constraint checks are performed and Interpolated Response Surfaces (IRS) are created for the constraints and objective functions. Optimization and IRS model refinement are then performed on these IRS models and the final optimum geometry and design vector are output. As an alternate to IRS model optimization and refinement, a direct driven approach is also provided wherein design variable sensitivities are directly calculated from calls to the flow solver, rather than to an IRS model.

Once initial user inputs have been completed the system can proceed in an automated fashion. Parallelization of the optimization process has been implemented within most domains providing a capability to utilize large scale, multiple CPU computing platforms in a computationally efficient manner. The Inter-domain Communication Facility (ICF) maintains the underlying process control (Ref.^[21]). It is constructed using TCL1 scripts, the MICO2 CORBA Orb and the Combat3 TCL to CORBA4 Bridge. Transfer of user input information is achieved through a master namelist file and parser utilities that extract or modify namelist parameter definitions as needed throughout the process. This namelist file also acts as the conduit between the GUI, the ICF, the Database Management Facility (DMF) and the discipline domain control scripts. All persistent user data, i.e. data created by the system, are stored into a MDOPT database via DMF utilities and MySQL5, with the exception of large binary computational model files (e.g. flow solver restart files) which are maintained separately within the system directory structure.

1. CFD Driver

The NASA Langley Research Center developed Navier-Stokes solver TLNS3D (Ref.[²²]), available as an option in the MDOPT aerodynamics domain, is used in the present study. Thin layer Reynolds averaged Navier-Stokes equations are solved using a five stage Runge-Kutta time integration scheme. A finite volume scheme based on Jameson's approach Ref.[²³] is employed to construct both viscous and inviscid fluxes. Matrix dissipation is added to enhance numerical stability, and a multigrid scheme is used to accelerate convergence rate. Although several turbulence models are available in the code the Spalart-Almaras (SA) model was used throughout this analysis. The entire flow field is treated as fully turbulent. A robust, reliable, accurate and fast method is desirable for optimization calculations and TLNS3D seems to fit the bill, especially for geometries that can be gridded with a simple single block grid.

Lift, drag and pitching moment convergence for the baseline solution on a 3,582,225 point grid with TLNS3D run in lift matching mode was obtained in 300 iterations, or approximately 3 hours running on a single 2.6 GHz OPTERON processor. Converged solutions on the perturbed geometries, also in lift matching mode, were obtained from restarting the baseline solution in 200 iterations or 2 hours. The optimizations were run on an in-house cluster of dual node OPTERON processors with 4 GB RAM each, and with as many as 48 solutions running in parallel during times of low cluster usage.

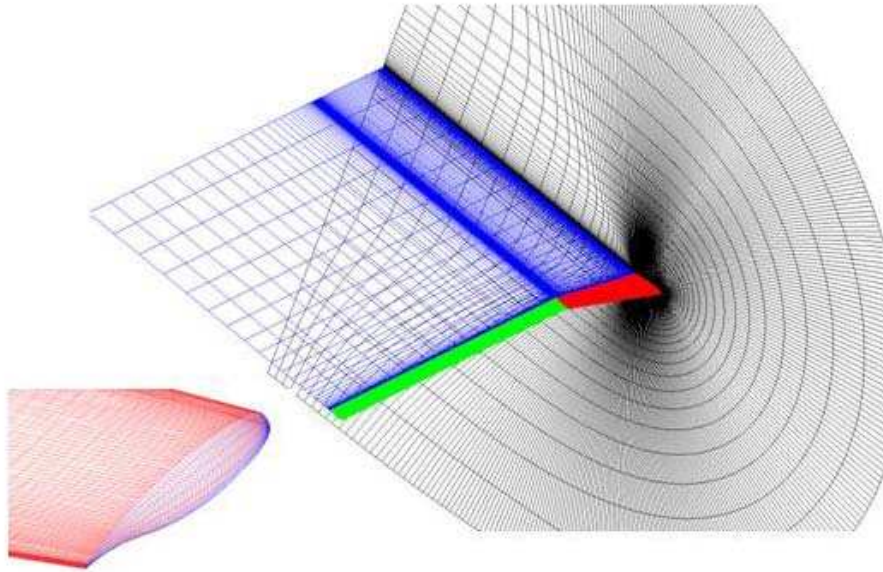


Figure 2. A single block C-H volume grid topology for TLNS3D computations.

The baseline wing surface grid was taken from the OVERFLOW analysis (described in Section V, Subsection D) up to the reference wing tip. The tip was closed by an in-house method that generates a rounded closed tip with maximum radius equal to half the wing tip thickness and adds 5 spanwise grid planes. Surface perturbations for each design point are calculated by routines within MDOPT. A single block C-H volume grid topology is used with 41 axial points in the wing trailing wake and 41 spanwise points from the wing tip to the far field (see Fig. 2). The wing wake is closed at the first point off the wing surface and no grid points are located along the blunt trailing edge. It was shown that this handling of the

wake grid in a single block grid gives the most similar solution to a full multiblock OVERFLOW solution with grid on the blunt trailing edge. The downstream far field is located at about 12.5 reference chord lengths aft of the wing trailing edge and the spanwise far field is at approximately 3.3 reference span lengths outboard of the wing tip. The baseline volume grid is generated by LEGRID (A variant of HYPGEN Ref.[²⁴]) and the perturbed geometry volume grids are generated by CSCMDO Ref.[²⁵], both are within the MDOPT framework. There are 81 points normal to the surface clustered for a boundary layer at the design Reynolds Number with the far field at approximately 12.5 reference chord lengths from the surface. There are 225 points around the wing airfoil surface and the wing tip is at the 105th spanwise plane. The full volume grid consists of 3,582,225 points, with dimensions of (305x145x81).

2. Design Variables

Design variables were chosen for this study to give as much flexibility to the solution as possible and to ease the resolution of geometric constraints. In total, 35 design variables were maintained throughout the study for consistency. Each design variable was constrained by its minimum and maximum values; however, never in any of the optimizations did an optimum result with any of the design variables at their extremes. The minimum and maximum values were chosen, for the most part, as + or - 20% of the baseline value for each design variable in order to assure some degree of reasonableness in the resulting geometries. These values are perturbations added to the baseline geometry, and as such the baseline design vector consists of 35 zeros.

There are 4 design stations, nominally the root, the tip and 40% and 75% span. Twist is varied independently at each of the three most outboard design stations. Minimum and maximum values were chosen for reasonableness.

Camber and thickness perturbation splines are specified at each of the design stations and are given as fraction of chord. Each spline is defined by three knots located at 25% 47.5% and 75% chord. There are also two implied knots at 0% and 100% chord where the perturbation is zero. The minimum value of the thickness spline at 25% and 75% chord is set to zero in order to satisfy the spar thickness constraint. Thus, the thickness at these two chord locations can never be less than the baseline.

In order to give the designer more control over leading and trailing edge camber, a leading edge and trailing edge deflection design variable is given at each design station in degrees. The leading edge “hinge line” is at 10% chord and the trailing edge “hinge line” is at 85% chord. Minimum and maximum values were chosen for reasonableness.

C. Optimization Tool OPTIMAS

The optimization tool OPTIMAS uses Genetic Algorithm as its search engine. Genetic Algorithms became highly popular as optimization methods in the last two decades. The basic idea behind Genetic Algorithms is to mathematically imitate the evolution process of nature. They are semi-stochastic optimization methods that are conveniently presented using the metaphor of natural evolution: a randomly initialized population of individuals (set of points of the search space at hand) evolves following a crude parody of the Darwinian principle of the survival of the fittest. The main point is that the probability of survival of new individuals depends on their fitness: the best are kept with a high probability, the worst are rapidly discarded.

As a basic algorithm, a variant of the floating-point GA is employed Ref.[26]. We used the tournament selection, which enables us to increase the diversity of the parents. Three types of the crossover operator have been employed: single point, uniform and arithmetical crossover. As the mutation operator we applied the non-uniform mutation.

In the present work the shape of the wing is defined as follows:

- A) Planform of the configuration is fixed.
- B) The wing surface is generated by a linear spanwise interpolation between 2D sectional cuts.
- C) The number of the wing sections N_{ws} is fixed.
- D) Shape of the 2D cuts is determined by Bezier Splines.

For the geometry description the absolute Cartesian coordinate system (x, y, z) is used, where the axes x and z are directed along the streamwise and spanwise direction, respectively.

The planform is defined by the following parameters: the length c_1 at the symmetry plane $z = 0$, span location of the streamwise sections $\{z_i\}$ and the corresponding leading and trailing edge sweep angles ($\{\lambda_i^{le}\}$ and $\{\lambda_i^{tr}\}$).

For each spanwise section, the non-dimensional shape is defined in a local Cartesian coordinate system (\bar{x}, \bar{y}) in the following way. The coordinates of the leading edge and trailing edge are respectively $(0, 0)$ and $(1, 0)$. For approximation of the upper and lower cut surface, Bezier Spline representations are used.

Finally, the shape of a sectional cut is completely determined by a total of $2N - 5$ parameters $(a_1, a_2, \dots, a_{N-1}, a_N, \dots, a_{2N-5})$, where N is the order of Bezier curve.

In order to fully specify the configuration shape it is necessary to set locations of the 2D sectional cuts in addition to their shapes. Assuming that the chord value and the trailing edge location are defined by the planform, sectional locations are specified by means of two additional design parameters per section: twist angle $\{\alpha_i^{tw}\}$ and dihedral value $\{\gamma_i^{dh}\}$. Note that for the root wing section these values are set to zero. Summing up, the set of design parameters consists of Bezier spline coefficients, twist angle and dihedral value for all design sections.

The problem of optimization of aerodynamic shapes is very time-consuming as it requires a huge amount of computational work. Each optimization step requires a large number of lengthy CFD runs, and a number of such steps is needed to reach the optimum.

Thus the construction of a computationally efficient algorithm is vital for the success of the method in an engineering environment. To reach this goal the following multilevel parallelization strategy was employed Ref. [27]:

- Level 1 - Parallelization of full Navier-Stokes solver
- Level 2 - Parallel evaluation of objective function
- Level 3 - Parallelization of the optimization framework

As a gas-dynamic model for calculating C_D and C_L values, the full Navier-Stokes equations are used. Numerical solution of the full Navier-Stokes equations was based on the code NES (Ref. [28–30]) which employs the Essentially Non-Oscillatory (ENO) concept with a flux interpolation technique which allows accurate estimation of sensitive aerodynamic characteristic such as lift, pressure drag, friction drag and pitching moment.

To accelerate the convergence to the steady-state, a defect correction multigrid approach is used which employs a first-order-accurate driver and a high-order ENO defect correction. Non-linear stability is maintained via approximation of inviscid fluxes on a variable template according to local characteristics and smoothness of the fluxes; viscous fluxes are approximated in a straightforward way. The resulting

multigrid method retained the high accuracy of the ENO approach with comparatively small number of multigrid cycles needed to reduce the error below the level of truncation errors.

The important advantage of the solver NES as a driver of optimization process is its ability to supply reliable and sufficiently accurate results even on relatively coarse meshes and thus to reduce dramatically the volume of CFD computations.

More details concerning the tool OPTIMAS may be found in Ref. [7] and Ref. [31], where the aerodynamic design of 3D isolated transport-type wings was presented.

V. Analysis of Results

A. SYN107 Results

A total of 6 optimizations have been performed. The design conditions and constraints are summarized in Table 1. The corresponding optimal shapes are designated by *Case_S1* to *Case_S6*. The first 3 test cases deal with optimizations unconstrained with respect to C_M while the last 3 test cases performed included the pseudo trim-drag penalty. The thicknesses of the optimal wings were everywhere greater than or equal to the original wing's thickness.

The results of optimization were verified through Navier-Stokes computations by the code FLO107. The computational grids contained 4 multigrid levels. Each level included either 8 or 12 blocks, depending on the computer. The total number of grid points in the fine level mesh was 818,545. The results of flow analysis in terms of the absolute values of C_D and C_M at $C_L = 0.5$ for $M = 0.76$ and $M = 0.78$ are presented in Table 2.

| Case No. | C_L^* | M | <i>beam</i> | C_M^* |
|----------------|---------|------|-------------|--------------|
| <i>Case_S1</i> | 0.50 | 0.76 | yes | $-\infty$ |
| <i>Case_S2</i> | 0.50 | 0.78 | yes | $-\infty$ |
| <i>Case_S3</i> | 0.50 | 0.76 | yes | $-\infty$ |
| | 0.50 | 0.77 | yes | $-\infty$ |
| | 0.50 | 0.78 | yes | $-\infty$ |
| <i>Case_S4</i> | 0.50 | 0.76 | yes | C_M^{orig} |
| <i>Case_S5</i> | 0.50 | 0.78 | yes | C_M^{orig} |
| <i>Case_S6</i> | 0.50 | 0.76 | yes | C_M^{orig} |
| | 0.50 | 0.77 | yes | C_M^{orig} |
| | 0.50 | 0.78 | yes | C_M^{orig} |

Table 1. DPW-W1 wing alone. SYN107: Optimization conditions and constraints.

The first optimization *Case_S1* was a one-point optimization at the main design point ($M = 0.76$, $C_L = 0.5$), the second optimization *Case_S2* was a one-point optimization at ($M = 0.78$, $C_L = 0.5$), while the third one *Case_S3* was a three-point optimization ($M = 0.76$, $M = 0.77$, $M = 0.78$, $C_L = 0.5$).

The corresponding surface pressure comparisons between the original geometry and the optimal one are presented in Fig.3-5. It can be observed that the one-point optimization yields virtually shockless pressure distributions.

The graphical data which illustrate the results of multipoint optimization *Case_S3* are shown in Fig.6-8.

Results of the optimizations which were penalized with respect to C_M (*Case_S4*

| Case No. | M=0.76 | M=0.78 | M=0.76 | M=0.78 |
|-----------------|---------|---------|----------|----------|
| | C_D | C_D | C_M | C_M |
| <i>DPW - W1</i> | 222.3 c | 244.9 c | - 0.0734 | - 0.0834 |
| <i>Case_S4</i> | 209.4 c | 241.9 c | - 0.0669 | - 0.0764 |
| <i>Case_S5</i> | 218.6 c | 215.1 c | - 0.0771 | - 0.0842 |
| <i>Case_S6</i> | 211.8 c | 218.6 c | - 0.0750 | - 0.0834 |

Table 2. Original DPW-W1 wing vs. optimal geometries achieved by the optimization tool SYN107. Estimation of C_D and C_M by the code FLO107.

- *Case_S6*) were as follows. The one-point optimization *Case_S4* (design Mach $M = 0.76$) yielded drag reduction of 12.9 aerodynamic counts, while at an off-design Mach $M = 0.78$, the drag reduction was equal to 3.0 counts. In turn the one-point optimization at the design Mach $M = 0.78$ (*Case_S5*) reduced the original drag value by 29.8 counts, while at an off-design $M = 0.76$ the corresponding drag reduction was equal to 3.7 counts. The three-point optimization *Case_S6* reduced the total drag by 10.5 counts at $M = 0.76$ and by 26.3 counts at $M = 0.78$. Interestingly, if one adds the 12.9 count improvement of *Case_S4* with the 29.8 count benefit of *Case_S5*, a threshold level of 42.7 counts is established. This level represents an upper bound to the aggregate improvement that can be achieved by a multipoint design at these two flow conditions. The aggregate improvement from *Case_S6* is 36.8 counts. Hence, this multipoint optimization recovered over 86% of its maximum potential improvement.

B. MDOPT Results

A total of 8 optimizations have been performed. The design conditions and constraints are summarized in Table 3. The corresponding optimal shapes are designated by *Case_M1* to *Case_M9*. *Case_M1* - *Case_M5* deal with one-point optimization at the design Mach $M = 0.76$, while *Case_M6* - *Case_M9* performed dual-point optimization. All cases include the spar thickness constraints at $x/c = 0.2$ and 0.75 , as described in the design variable section above, and all constrain the maximum airfoil thickness to be no less than the baseline. Several cases include a penalty in the cost function, C_D^{cor} for increasing the nose down pitching moment. The cost function for the other cases is simply the drag coefficient, C_D . Some cases were run with sequential response surface model optimization and refinement, SEQOPT, while others were run with a direct driven, DD, optimization scheme.

The results of optimization were verified through Navier-Stokes computations by the code TLNS3D. The total number of points in the fine level was about 3,582,225. The results of flow analyses in terms of the absolute values of C_D and C_M at $C_L = 0.5$ for $M = 0.76$ and $M = 0.78$ are presented in Table 4.

Case_M1 was basically a shakeout run to get the MDOPT system working efficiently on our compute cluster and to determine the best settings for various parameters that control the optimization and model refinements. This first case therefore took an inordinate amount of time to complete. It achieved an 11.8 count improvement over the baseline but with significant increase in nose down pitching moment. When the nose down pitching moment penalty is included in the cost function, *Case_M5* was able to achieve the same amount of drag reduction as *Case_M1* did, however, it did so with less nose-down pitching moment.

It should be noted that these two cases only differ with respect to the optimization method and the reason that *Case_M4* did not reach the level of *Case_M5* drag

| Case No. | C_L^* | M | $beam$ | C_M^* | opt. type | # runs | CPU days |
|-----------------|---------|------|--------|--------------|-----------|--------|----------|
| <i>Case_M1</i> | 0.50 | 0.76 | yes | $-\infty$ | SEQ | 1404 | 26 |
| <i>Case_M4</i> | 0.50 | 0.76 | yes | C_M^{orig} | SEQ | 732 | 10 |
| <i>Case_M5</i> | 0.50 | 0.76 | yes | C_M^{orig} | DD | 412 | 6 |
| <i>Case_M6</i> | 0.50 | 0.76 | yes | $-\infty$ | DD | 862 | 9 |
| | 0.50 | 0.78 | yes | $-\infty$ | | | |
| <i>Case_M7</i> | 0.50 | 0.76 | yes | C_M^{orig} | DD | 1030 | 18 |
| | 0.50 | 0.78 | yes | C_M^{orig} | | | |
| <i>Case_M8</i> | 0.50 | 0.76 | yes | $-\infty$ | SEQ | 1986 | 10 |
| | 0.50 | 0.78 | yes | $-\infty$ | | | |
| <i>Case_M8A</i> | 0.50 | 0.76 | yes | $-\infty$ | SEQ | 1214 | 4 |
| | 0.50 | 0.78 | yes | $-\infty$ | | | |
| <i>Case_M9</i> | 0.50 | 0.76 | yes | C_M^{orig} | SEQ | 2676 | 14 |
| | 0.50 | 0.78 | yes | C_M^{orig} | | | |

Table 3. DPW-W1 wing alone. MDOPT: Optimization conditions and constraints.

| Case No. | M=0.76 | M=0.78 | M=0.76 | M=0.78 |
|-----------------|---------|---------|----------|----------|
| | C_D | C_D | C_M | C_M |
| <i>DPW – W1</i> | 223.1 c | 247.6 c | - 0.0714 | - 0.0812 |
| <i>Case_M1</i> | 211.3 c | | - 0.0889 | |
| <i>Case_M4</i> | 213.1 c | | - 0.0707 | |
| <i>Case_M5</i> | 211.4 c | 241.5 c | - 0.0784 | - 0.0867 |
| <i>Case_M6</i> | 215.7 c | 220.0 c | - 0.1159 | - 0.1240 |
| <i>Case_M7</i> | 216.0 c | 219.6 c | - 0.1000 | - 0.1071 |

Table 4. Original DPW-W1 wing vs. optimal geometries achieved by the optimization tool MDOPT. Estimation of C_D and C_M by the code TLNS3D.

reduction is that it was stopped prematurely and was still headed towards increased drag improvement, as Fig. 9 shows. Generally it takes twice as many flow code evaluations for the SEQOPT cases compared to the Direct Driven cases to reach an optimum; however the time to get a final solution is comparable because more of the flow code evaluations in SEQOPT can be run in parallel.

Fig. 11 - 10 show a comparison of the resulting pressure distributions and spanloads for *Case_M1* and *Case_M5* compared to the baseline. MDOPT was successful in significantly reducing the shock strength as well as moving the spanload outward for a wave and induced drag benefit. The effect of the pitching moment penalty did not allow the spanload to move outboard as much as for *Case_M1* and each sectional pressure distribution shows a tendency towards less nose-down moment.

Case_M6, *Case_M8* and *Case_M8A* are multi-point designs without any pitching moment penalty included in the cost function, i.e., drag. These cases were run with SEQOPT and the Direct Driven optimizer, and *Case_M8A* is a rerun of *Case_M8* starting from the final refined response surface from *Case_M8*.

Once again these cases stress the importance of achieving a well converged solution. With the SEQOPT method in particular, which tends to find improvements in a stepwise manner, it is particularly prudent to let it run for a significant number of cycles past what one might think is a converged solution. It is possible for it to find a better local minimum and step to it as the response surface model is refined.

None of these cases were able to reach the drag improvement achieved by the single point design, *Case_M1*, at $M = 0.76$. The optimization chose to sacrifice almost 3 counts of drag at the lower Mach number to reduce the drag at the higher Mach number by about 30 counts.

The two multi-point design cases with pitching moment penalty used in the cost function, *Case_M7* and *Case_M9*, differ by the starting geometry. *Case_M7* starts from the baseline, while *Case_M9* starts from the resulting geometry of *Case_M5* in order to determine if it is possible to reach the single point optimum at the lower Mach number.

At both Mach numbers, the decrease in drag and drag corrected for pitching moment are better than or equal to the cases with no pitching moment penalty. It is also noted that the single point optimum at the lower Mach number is not achieved. The pressure distributions in Fig. 12 - 15 show that for both cases the shock strength at the lower Mach number was not as successfully reduced as in the single point optimization; however, significant improvement is seen at the higher Mach. At the higher Mach, MDOPT seems to have traded a strong shock at the wing tip with two weaker shocks.

This double shock behavior is intuitively undesirable and may leave room for additional improvement. MDOPT may have been limited in this sense by the choice of design variables which may have constricted the changes desired near the tip. Both cases show an outboard shifting of the spanload at both Mach numbers as in the single point optimization cases, indicative of an induced drag benefit.

Cases_M8 - M9 represent the beginning of a follow-on activity to the present work, and will be documented in further detail in a sequel paper after the authors have the opportunity to cross-analyze these geometries with each other's CFD methods.

C. OPTIMAS Results

We present here applications of the the tool OPTIMAS to the solution of the above specified test-cases. A total of 8 optimizations have been performed. The design conditions and constraints are summarized in Table 5. The corresponding optimal shapes are designated by *Case_O1* to *Case_O8*.

The design problem consists of the minimization of total drag starting from the original wing at the above design points. The average number of optimization steps needed to reach convergence was equal to 8. On the computer cluster with 108 processors, it took about 16 wall clock hours.

The results of optimization were verified through Navier-Stokes computations by the code NES. The computational grids contained three multigrid levels. Each level included 4 blocks. The total number of points in the fine level was about 250,000. The results of flow analysis in terms of the absolute values of C_D and C_M at $C_L = 0.5$ for $M = 0.76$ and $M = 0.78$ are presented in Table 6.

Before analyzing the results of the optimizations, let us consider the systematic comparison between NES data and OVERFLOW data for the same geometries at the main design point $M = 0.76$, $C_L = 0.5$. The corresponding comparison is given in Table 7 for the values of viscous drag C_D^{visc} , pressure drag C_D^{pres} and total drag C_D computed by the code NES and the code OVERFLOW. It may be concluded, that the two codes yield very similar drag results in terms of both viscous and pressure drag for a wide range of tested geometries. Specifically, on the average the difference between C_D values by these two codes is about 1 count.

At the main design point the drag of the original wing is 217.8 aerodynamic counts, while the corresponding drag value for *Case_O1* amounts to 199.7 counts ($C_M = -0.129$ compared to the original -0.071). The corresponding pressure distributions on the upper surface of the original wing and the optimized one for *Case_O1* are presented in Fig.16-17.

The incorporation of the pitching moment constraint (*Case_O2*) increases the drag value by only 0.6 counts ($C_D = 200.3$ counts, $C_M = -0.071$). In comparison with *Case_O1*, it can be seen that, in accordance with aerodynamic common sense, the imposition of a constraint on C_M redistributes the pressure by increasing the loading in the leading edge area.

A detailed analysis of the results allows us to conclude that both of the optimized wings feature shockless behaviour. Note, that the corresponding drag values are very close to the theoretical minimum ($C_{D_0} + C_D^{induced}$).

In order to check off-design behaviour of the optimized geometries, accurate full Navier-Stokes computations were performed for a wide range of free-stream Mach and C_L values. The corresponding results are given in Fig.18-19, where lift/drag polars at $M = 0.76$ and Mach drag rise curves at $C_L = 0.5$, respectively, are depicted.

It is seen that the optimized wings possess significantly lower drag values, not only pointwise, but also for all $C_L > 0.2$. The optimization also improved the M_{DD} behaviour of the wings and shifted the divergence to a higher Mach number.

Both optimized wings have similar lift/drag performance at the transonic flight conditions. At the same time the corresponding optimal shapes (see Fig.20-22) are markedly different. This indicates that the optimization problem considered here was not well posed.

Another 3 cases deal with one-point optimizations for different Mach design values which include constraints on local thickness of the wing sections (beam constraints): *Case_O3* (unconstrained C_M , $M = 0.76$), *Case_O4* (constrained C_M , $M=0.76$) and *Case_O6* (constrained C_M , $M=0.78$).

In *Case_O3* the optimization yielded 200.7 drag counts ($C_M=-0.129$), in *Case_O4* the total drag was equal to 204.3 counts while the pitching moment was kept to the original level ($C_M=-0.071$). It is seen, that the penalty due to beam constraints depends on the constraints on C_M values. In the unconstrained optimization the drag increases by only 1 count, while in the constrained pitching moment case the penalty is higher (4 counts), although remaining relatively low.

The corresponding lift/drag and M_{DD} curves are shown in Fig.23-24 while the comparisons of the optimal shapes with the original one are presented in Fig.25-27.

| Case No. | C_L^* | M | <i>beam</i> | C_M^* |
|----------------|---------|------|-------------|-----------|
| <i>Case_O1</i> | 0.50 | 0.76 | no | $-\infty$ |
| <i>Case_O2</i> | 0.50 | 0.76 | no | -0.071 |
| <i>Case_O3</i> | 0.50 | 0.76 | yes | $-\infty$ |
| <i>Case_O4</i> | 0.50 | 0.76 | yes | -0.071 |
| <i>Case_O5</i> | 0.50 | 0.76 | yes | -0.071 |
| | 0.50 | 0.78 | yes | $-\infty$ |
| | 1.80 | 0.20 | yes | $-\infty$ |
| <i>Case_O6</i> | 0.50 | 0.78 | yes | -0.081 |
| <i>Case_O7</i> | 0.50 | 0.76 | yes | -0.071 |
| | 0.50 | 0.78 | yes | $-\infty$ |
| <i>Case_O8</i> | 0.50 | 0.76 | yes | $-\infty$ |
| | 0.50 | 0.78 | yes | $-\infty$ |

Table 5. DPW-W1 wing alone. OPTIMAS: Optimization conditions and constraints.

It can be concluded that the optimization tool allowed the successful incorporation of beam constraints in both cases.

| Case No. | M=0.76 | M=0.78 | M=0.76 | M=0.78 |
|-----------------|---------|---------|---------|---------|
| | C_D | C_D | C_M | C_M |
| <i>DPW – W1</i> | 217.8 c | 241.3 c | - 0.071 | - 0.081 |
| <i>Case_O1</i> | 199.7 c | 220.0 c | - 0.129 | - 0.138 |
| <i>Case_O2</i> | 200.3 c | 220.6 c | - 0.071 | - 0.082 |
| <i>Case_O3</i> | 200.7 c | 221.0 c | - 0.129 | - 0.139 |
| <i>Case_O4</i> | 204.3 c | 226.7 c | - 0.071 | - 0.081 |
| <i>Case_O5</i> | 203.6 c | 220.5 c | - 0.071 | - 0.081 |

Table 6. Original DPW-W1 wing vs. optimal geometries achieved by the optimization tool OPTIMAS. Estimation of C_D and C_M by the code NES.

Finally we present the results of a three-point optimization *Case_O5*. At the main design point ($M = 0.76$, $C_L = 0.50$) the total drag of the optimized wing for *Case_O5* was equal to 203.6 counts, while the pitching moment was kept to the original level. At the high Mach secondary design point ($M = 0.78$, $C_L = 0.50$) the resulting C_D was equal to 220.5 aerodynamic counts (compared to the original 241.3 counts). At the take-off secondary design condition the optimization preserved the original value of C_L^{max} at $M = 0.20$.

The pressure distribution for *Case_O5* at $M = 0.76$, $C_L = 0.50$ is given in Fig.28, while the corresponding data at $M = 0.78$, $C_L = 0.50$ for *Case_O5* and for the original wing are given in Fig.29-30. The data illustrating the aerodynamic performance of the optimized wing (lift/drag curves, MDD and C_L vs. angle of attack curves) are shown in Fig.31-34, while the shape comparisons are presented in Fig.35-37.

The last 3 optimizations *Case_O6*–*Case_O8* represent the beginning of a follow-on activity to the present work, and will be documented in further detail in a sequel paper after the authors have the opportunity to cross-analyze these geometries with

| Geometry | NES | NES | NES | OVERFLOW | OVERFLOW | OVERFLOW |
|-----------------|--------------|--------------|-------|--------------|--------------|----------|
| | C_D^{visc} | C_D^{pres} | C_D | C_D^{visc} | C_D^{pres} | C_D |
| <i>DPW – W1</i> | 57.3 | 160.5 | 217.8 | 59.3 | 160.0 | 219.3 |
| <i>Case_O1</i> | 58.1 | 141.6 | 199.7 | 60.5 | 140.3 | 200.8 |
| <i>Case_O2</i> | 58.3 | 142.0 | 200.3 | 60.8 | 141.8 | 202.6 |
| <i>Case_O3</i> | 58.4 | 142.4 | 200.7 | 60.7 | 140.6 | 201.3 |
| <i>Case_O4</i> | 58.3 | 145.9 | 204.3 | 60.7 | 143.8 | 204.5 |
| <i>Case_O5</i> | 58.2 | 145.4 | 203.6 | 60.7 | 142.5 | 203.2 |

Table 7. Original DPW-W1 wing and optimal geometries achieved by the optimization tool OPTIMAS. Drag values at $M = 0.76$, $C_L = 0.5$ in aerodynamic counts. NES computations vs. OVERFLOW ones.

each other’s CFD methods.

D. Cross-Analysis of Optimal Wings

A systematic cross-analysis was performed for the original geometry and several optimal geometries generated by the optimization tools **SYN107**, **MDOPT** and **OPTIMAS**. These geometries are from cases which best match the single-point and multi-point optimizations outlined in Section III of this paper, and which were performed independent of knowledge of each of the other group’s results. In total 4 different Navier-Stokes solvers were used in this verification study: the code TLNS3D (the CFD driver of the optimization tool **MDOPT**), the code FLO107 (**SYN107**), the code NES (**OPTIMAS**) and the code OVERFLOW.

CFD solutions using the NASA code OVERFLOW were used in order to provide an unbiased comparative analysis (relative to the optimizers’ own solutions) of the optimized geometries. OVERFLOW [32] is a node-based Reynolds-Averaged Navier-Stokes flow solver that can calculate solutions of complex geometries by using multiple structured, overset grid topologies. The Boeing solutions were generated using the Message-Passing-Interface (MPI) version 2.0z OVERFLOW, with 64-bit precision, and grid sequencing for accelerated convergence. The one-equation Spalart-Allmaras [33] turbulence model was used, and the solutions did not incorporate the thin-layer approximations. A 2nd order Roe upwind numerical differencing scheme was used.

| Solver | M=0.76 | M=0.78 | M=0.76 | M=0.78 |
|-----------------|---------|---------|----------|----------|
| | C_D | C_D | C_M | C_M |
| <i>FLO107</i> | 222.3 c | 244.9 c | - 0.0734 | - 0.0834 |
| <i>TLNS3D</i> | 223.1 c | 247.6 c | - 0.0714 | - 0.0812 |
| <i>NES</i> | 217.8 c | 241.3 c | - 0.0710 | - 0.0810 |
| <i>OVERFLOW</i> | 220.3 c | 247.0 c | - 0.0660 | - 0.0740 |

Table 8. The original geometry DPW-W1 wing alone. Estimation of C_D and C_M by the different Navier-Stokes solvers.

Solutions for the DPW-W1 [34] and optimized geometry solutions utilized a three-block grid topology comprised of a wing grid, trailing edge cap grid, and wing tip cap grid. Total grid point count for the computational domain was approxi-

mately 4 million nodes. All surface and volume grid construction practices were in accordance with the methods outlined by Vassberg [35]. Near-wall y^+ spacing of 1 was maintained for all viscous wall grids. Wing surface grid chordwise spacing was clustered to a length of 0.1% local chord at both the leading and trailing edges. The wing grid was coupled with a wake that extended downstream a distance equal to the wing reference chord. The total wing-wake surface grid was comprised of 289 points in the streamwise direction, while the spanwise spacing had 101 total points. The wing trailing edge base was modified with an overset grid to incorporate a total of 13 chordwise cells and maintained the same spanwise spacing as the wing grid. The wingtip cap overset grid maintained the wing grid streamwise point spacing, and closed out the tip by rounding the wing surface over and collapsing the constant-k grid planes. The outer computational boundaries were placed away from the wing grid at a distance equal to 35 times the reference chord length.

| | M=0.76 | M=0.78 | M=0.76 | M=0.78 |
|----------------|--------------|--------------|--------------|--------------|
| Case No. | ΔC_D | ΔC_D | ΔC_M | ΔC_M |
| <i>Case_S4</i> | - 12.9 c | - 3.0 c | + 0.0065 | + 0.007 |
| <i>Case_S5</i> | - 3.7 c | - 29.8 c | - 0.0037 | - 0.001 |
| <i>Case_S6</i> | - 10.5 c | - 26.3 c | - 0.002 | + 0.0001 |
| <i>Case_M5</i> | - 11.0 c | - 6.0 c | - 0.0064 | - 0.0055 |
| <i>Case_M7</i> | - 6.5 c | - 25.2 c | - 0.028 | - 0.025 |
| <i>Case_O4</i> | - 13.9 c | - 15.0 c | - 0.009 | - 0.0085 |
| <i>Case_O5</i> | - 13.8 c | - 20.4 c | - 0.011 | - 0.010 |

Table 9. Estimation of drag reduction by the code FLO107.

| | M=0.76 | M=0.78 | M=0.76 | M=0.78 |
|----------------|--------------|--------------|--------------|--------------|
| Case No. | ΔC_D | ΔC_D | ΔC_M | ΔC_M |
| <i>Case_S4</i> | - 13.2 c | - 2.8 c | + 0.004 | + 0.006 |
| <i>Case_S5</i> | - 3.4 c | - 31.3 c | - 0.005 | - 0.002 |
| <i>Case_S6</i> | - 10.4 c | - 27.6 c | - 0.004 | - 0.002 |
| <i>Case_M5</i> | - 11.7 c | - 6.1 c | - 0.007 | - 0.006 |
| <i>Case_M7</i> | - 7.1 c | - 28.0 c | - 0.029 | - 0.026 |
| <i>Case_O4</i> | - 16.6 c | - 19.5 c | - 0.006 | - 0.005 |
| <i>Case_O5</i> | - 17.4 c | - 25.4 c | - 0.008 | - 0.006 |

Table 10. Estimation of drag reduction by the code TLNS3D.

The corresponding results are presented in Tables 8-12 and in Fig. 38-44. Table 8 contains the results of flow analysis for the original geometry (in terms of absolute values of C_D and C_M); in Tables 9-12 we find the corresponding data for the optimal geometries (in terms of drag reduction), while chordwise pressure distributions (based on the OVERFLOW computations) on the optimal geometries at $M = 0.76$ and $M = 0.78$ are plotted in Fig. 38-41.

In order to compare the results of optimization achieved by the different optimization tools it was agreed to correct the actual drag reduction by the trim-drag penalty of 1 count per -0.01 in ΔC_M value, with no benefit incorporated if ΔC_M

| | M=0.76 | M=0.78 | M=0.76 | M=0.78 |
|----------------|--------------|--------------|--------------|--------------|
| Case No. | ΔC_D | ΔC_D | ΔC_M | ΔC_M |
| <i>Case_S4</i> | - 8.7 c | - 1.9 c | + 0.007 | + 0.008 |
| <i>Case_S5</i> | - 2.7 c | - 22.4 c | - 0.0001 | + 0.002 |
| <i>Case_S6</i> | - 5.7 c | - 19.2 c | + 0.001 | + 0.004 |
| <i>Case_M5</i> | - 10.0 c | - 3.9 c | - 0.002 | - 0.002 |
| <i>Case_M7</i> | - 8.4 c | - 28.7 c | - 0.020 | - 0.020 |
| <i>Case_O4</i> | - 13.5 c | - 14.7 c | + 0.0001 | - 0.002 |
| <i>Case_O5</i> | - 14.2 c | - 20.8 c | + 0.0001 | - 0.0001 |

Table 11. Estimation of drag reduction by the code NES.

| | M=0.76 | M=0.78 | M=0.76 | M=0.78 |
|----------------|--------------|--------------|--------------|--------------|
| Case No. | ΔC_D | ΔC_D | ΔC_M | ΔC_M |
| <i>Case_S4</i> | - 13.8 c | - 3.1 c | + 0.004 | + 0.006 |
| <i>Case_S5</i> | - 3.8 c | - 31.8 c | - 0.003 | - 0.001 |
| <i>Case_S6</i> | - 10.8 c | - 28.2 c | - 0.002 | - 0.001 |
| <i>Case_M5</i> | - 14.5 c | - 9.0 c | - 0.008 | - 0.005 |
| <i>Case_M7</i> | - 9.9 c | - 31.5 c | - 0.023 | - 0.021 |
| <i>Case_O4</i> | - 14.8 c | - 16.8 c | - 0.003 | - 0.002 |
| <i>Case_O5</i> | - 16.1 c | - 25.0 c | - 0.005 | - 0.003 |

Table 12. Estimation of drag reduction by the code OVERFLOW.

is positive. The corresponding bar charts with the corrected drag reduction values are presented in Fig. 42 and Fig. 43 (for $M = 0.76$ and $M = 0.78$, respectively).

Finally, in order to also estimate off-design behaviour of the optimized wings we introduced the aggregate drag reduction value, which is equal to the sum of ΔC_D achieved by an optimal geometry at $M = 0.76$ and $M = 0.78$ (corrected for trim-drag penalties). The corresponding bar charts with the corrected aggregate drag reduction values are presented in Fig. 44.

The analysis of the presented data shows that in general the drag reduction values estimated by different Navier-Stokes solvers correlated well for all the considered optimal geometries. Specifically, it can be concluded that, for all the considered optimization tools, the reduction in drag due to optimization calculated by each associated CFD analysis code was confirmed by the other Navier-Stokes solvers with sufficient accuracy.

VI. Conclusions

A comparative study of three CFD based optimization techniques applied to the solution of a 3D wing drag minimization problem was performed. As the starting geometry the public domain DPW-W1 wing (a test-case for the 3rd Drag Prediction Workshop) was used. The optimal geometries achieved by the aerodynamic design tools SYN107 (Intelligent Aerodynamics Int'l), MDOPT (The Boeing Company) and OPTIMAS (Israel Aerospace Industries) were systematically cross-checked by four Navier-Stokes solvers: FLO107, TLNS3D, NES and OVERFLOW. It can be concluded that the considered optimization tools allow the design of optimal shapes which satisfy aerodynamic and geometrical constraints, are aerodynamically feasible and yield essentially similar drag reductions at the main design point as well as good off-design performance.

References

- ¹Jameson, A., Martinelli, L. and Vassberg, J., "Using Computational Fluid Dynamics for Aerodynamics - A Critical Assessment". *ICAS Paper 2002-1.10.1*, Toronto, 2002.
- ²Obayashi, S., Yamaguchi, Y. and Nakamura, T., "Multiobjective Genetic Algorithm for Multidisciplinary Design of Transonic Wing Planform". *Journal of Aircraft*, **34**, 690–693, 1997.
- ³Mohammadi, B. and Pironneau, O., *Applied Shape Optimization for Fluids*, Oxford: Oxford University Press, 2001.
- ⁴Vassberg, J. and Jameson, A., "Aerodynamic Shape Optimization of a Reno Race Plane". *International Journal of Vehicle Design*, **28**, No.4, 318–338, 2002.
- ⁵Epstein, B., and Peigin, S., "Robust Hybrid Approach to Multiobjective Constrained Optimization in Aerodynamics", *AIAA Journal*, **42**, 1572–1581, 2004.
- ⁶Peigin, S. and Epstein, B., "Robust Handling of Non-Linear Constraints for GA Optimization of Aerodynamic Shapes". *Int. J. Numer. Meth. Fluids*, **45**, 1339–1362, 2004.
- ⁷Epstein, B., and Peigin, S., "Constrained Aerodynamic Optimization of Three-Dimensional Wings Driven by Navier-Stokes Computations", *AIAA Journal*, **43**, 1946–1957, 2005.
- ⁸Vassberg, J. and Jameson, A., "Aerodynamic Shape Optimization Part 1: Theoretical Background". von Karman Institute for Fluid Dynamics, Lecture Series - Introduction to Optimization and Multidisciplinary Design, Brussels, 2006.
- ⁹Vassberg, J. and Jameson, A., "Aerodynamic Shape Optimization Part 2: Sample Applications". von Karman Institute for Fluid Dynamics, Lecture Series - Introduction to Optimization and Multidisciplinary Design, Brussels, 2006.
- ¹⁰Jameson, A., "Optimum Aerodynamic Design Using Control Theory", *CFD Review*, 495–528, Wiley, 1995.
- ¹¹Jameson, A., "Aerodynamic Design via Control Theory", *Journal of Scientific Computing*, **3**, No.3, 233–260, 1988.
- ¹²Jameson, A., "Computational Aerodynamics for Aircraft Design", *Science*, **245**, 361–371, 1989.
- ¹³Jameson, A., "Optimum Aerodynamic Design Using CFD and Control Theory", 12th AIAA Computational Fluid Dynamics Conference, AIAA Paper 1995-1729.

- ¹⁴Jameson, A., Pierce, NA. and Martinelli, L., "Optimum Aerodynamic Design Using the Navier-Stokes Equations", *Theoretical and Computational Fluid Dynamics*, **10**, 213–237, 1998.
- ¹⁵Jameson, A. and Martinelli, L., "Aerodynamic Shape Optimization Techniques Based on Control Theory", *Lecture Notes in Mathematics*, **1739**, 2000.
- ¹⁶Jameson, A. and Vassberg, J., "Studies of Alternative Numerical Optimization Methods Applied to the Brachistotrone Problem", *Computational Fluid Dynamics Problem*, **9**, 281–296, 2000.
- ¹⁷Jameson, A. and Vassberg, J., "Computational Fluid Dynamics for Aerodynamic Design: Its Current and Future Impact", AIAA Paper 2001-0538, 2001.
- ¹⁸Leoviriyakit, K., Kim, S. and Jameson, A., "Aero-Structural Wing Planform Optimization Using the Navier-Stokes Equations", 10th AIAA/ISSMO Multidisciplinary Analysis and Optimization Conference, 30 August - 1 September 2004, Albany, New York, AIAA Paper 2004-4479.
- ¹⁹LeDoux, ST., Herling, WW., Fatta, J., Ratchiff, RR., "Multidisciplinary Design Optimization System Using Higher Order Analysis Code", 10th AIAA/ISSMO Multidisciplinary Analysis and Optimization Conference, 30 August - 1 September 2004, Albany, New York, AIAA Paper 2004-4567.
- ²⁰Audet, C., Dennis, J., Moore, D., Booker, A. and Frank, P., "Surrogate-Model-Based Method for Constrained Optimization", AIAA Multi-Disciplinary Optimization Conference, September 2000, AIAA Paper 2000-4891.
- ²¹Ratchiff, RR., LeDoux, ST., Herling, WW., "Modern CORBA-Based Approach to Ad Hoc Distributed Process Orchestrations Applied to MDO", Infotech@Aerospace, 26 - 29 September 2005, Arlington, Virginia, AIAA Paper 2005-7143.
- ²²Vatsa, VN. and Hammond, DP., "Viscous Flow Computations for Complex Geometries on Parallel Computers", 4th NASA Symposium on Large-scale Analysis and Design on High-performance Computers and Workstations, July 1997.
- ²³Jameson, A., "Multigrid Algorithms for Compressible Flow Calculations", 2nd European Conference on Multigrid Methods, Cologne, Oct. 1985.
- ²⁴Chan WM. and Steger, JL., "Enhancements of a Three-Dimensional Hyperbolic Grid Generation Scheme", *Applied Mathematics and Computing*, Vol. 51, 1992, pp.181–205.
- ²⁵Jones, WT. and Samareh-Abolhassani, J., "Grid Generation System for Multi-disciplinary Design Optimization", 12th AIAA Computational Fluid Dynamics Conference, June 20, 1995, San Diego, CA, AIAA Paper 1995-1689.
- ²⁶Michalewicz, Z., *Genetic Algorithms + Data Structures = Evolution Programs*, New-York: Springer Verlag, 1996
- ²⁷Peigin, S., and Epstein, B., "Embedded Parallelization Approach for Optimization in Aerodynamic Design", *The Journal of Supercomputing*, **29**, No. 3, 243–263, 2004.
- ²⁸Epstein, B., Rubin, T. and Seror, S., "Accurate Multiblock Navier-Stokes Solver for Complex Aerodynamic Configurations", *AIAA Journal*, **41**, 582–594, 2003.
- ²⁹Peigin, S., Epstein, B., Rubin, T., and Seror, S., "Parallel Large Scale High Accuracy Navier-Stokes Computations on Distributed Memory Clusters", *The Journal of Supercomputing*, **27**, 49–68, 2004.
- ³⁰Seror, S., Rubin, T., Peigin, S. and Epstein, B., "Implementation and Validation of the Spalart-Allmaras Turbulence Model for a Parallel CFD Code". *Journal of Aircraft*, **42**, 179–188, 2005
- ³¹Peigin, S., and Epstein, B., "Robust Drag Minimization of Aerodynamic Wings in Engineering Environment", *Journal of Aircraft*, **43**, No. 4, 1195–1204, 2006.
- ³²Buning, PG., Jespersen, DC., Pulliam, TH., Chan, WM., Slotnick, JP., Krist, SE. and Renze, KJ., "OVERFLOW user's manual, version 1.81", NASA Report, NASA Langley Research Center, Hampton, VA, 1999.
- ³³Spalart, PR. and Allmaras, SR., "A one-equation turbulence model for aerodynamic flows", *La Recherche Aerospaciale*, No. 1, 1994.
- ³⁴Sclafani, AJ., Vassberg, JC., Harrison, NA., DeHaan, MA., Rumsey, CL., Rivers, SM., Morrison, JH., "Drag Predictions for the DLR-F6 Wing/Body and DPW Wings using CFL3D and OVERFLOW on an Overset Mesh", 45th AIAA Aerospace Sciences Meeting and Exhibit, Reno, NV, January 2007, AIAA Paper 2007-0256.
- ³⁵Vassberg, JC., DeHaan, MA., Sclafani, AJ., "Grid Generation Requirements for Accurate Drag Predictions Based on OVERFLOW Calculations", 16th AIAA Computational Fluid Dynamics Conference, Orlando, FL, June 2003, AIAA Paper 2003-4124.

COMPARISON OF CHORDWISE PRESSURE DISTRIBUTIONS DPW-W1 WING (FLAT TIP AT Y=762.0)

REN = 6.43 , MACH = 0.760

| SYMBOL | SOURCE | ALPHA | CL | CD | CM |
|--------|------------------|-------|--------|---------|----------|
| — | SYN107P D.30 | 0.367 | 0.5011 | 0.02106 | -0.08896 |
| - - - | SYN107P Baseline | 0.565 | 0.5009 | 0.02226 | -0.07367 |

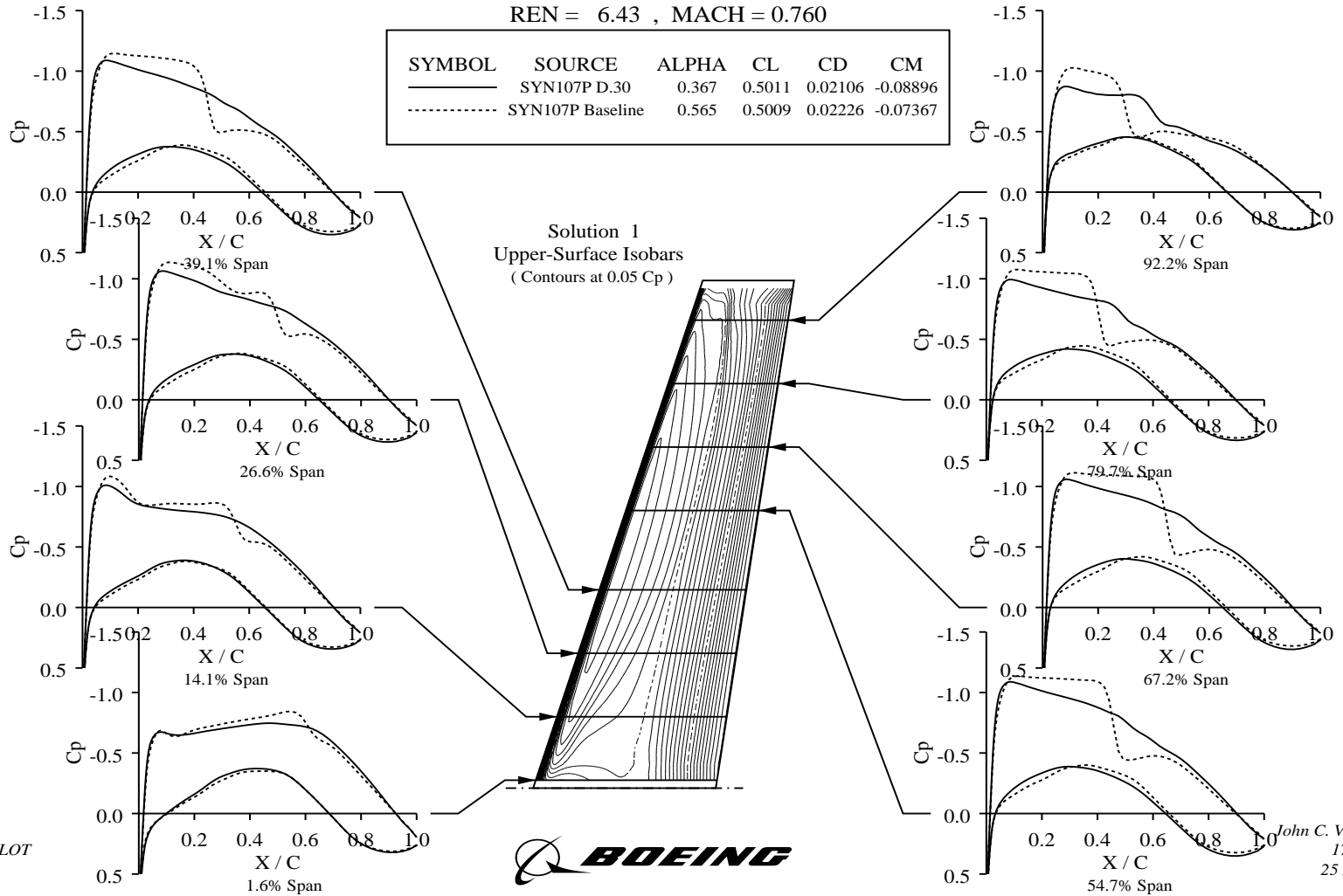


Figure 3. SYN107. One-point optimization Case-S1. Chordwise pressure distributions at $M = 0.76$, $C_L = 0.50$.

COMPPLOT
Ver 2.01

John C. Vassberg
17:33 Fri
25 May 07

COMPARISON OF UPPER SURFACE CONTOURS DPW-W1 WING (FLAT TIP AT Y=762.0)

REN = 5.00 , MACH = 0.760

(Contours at 0.05 Cp)

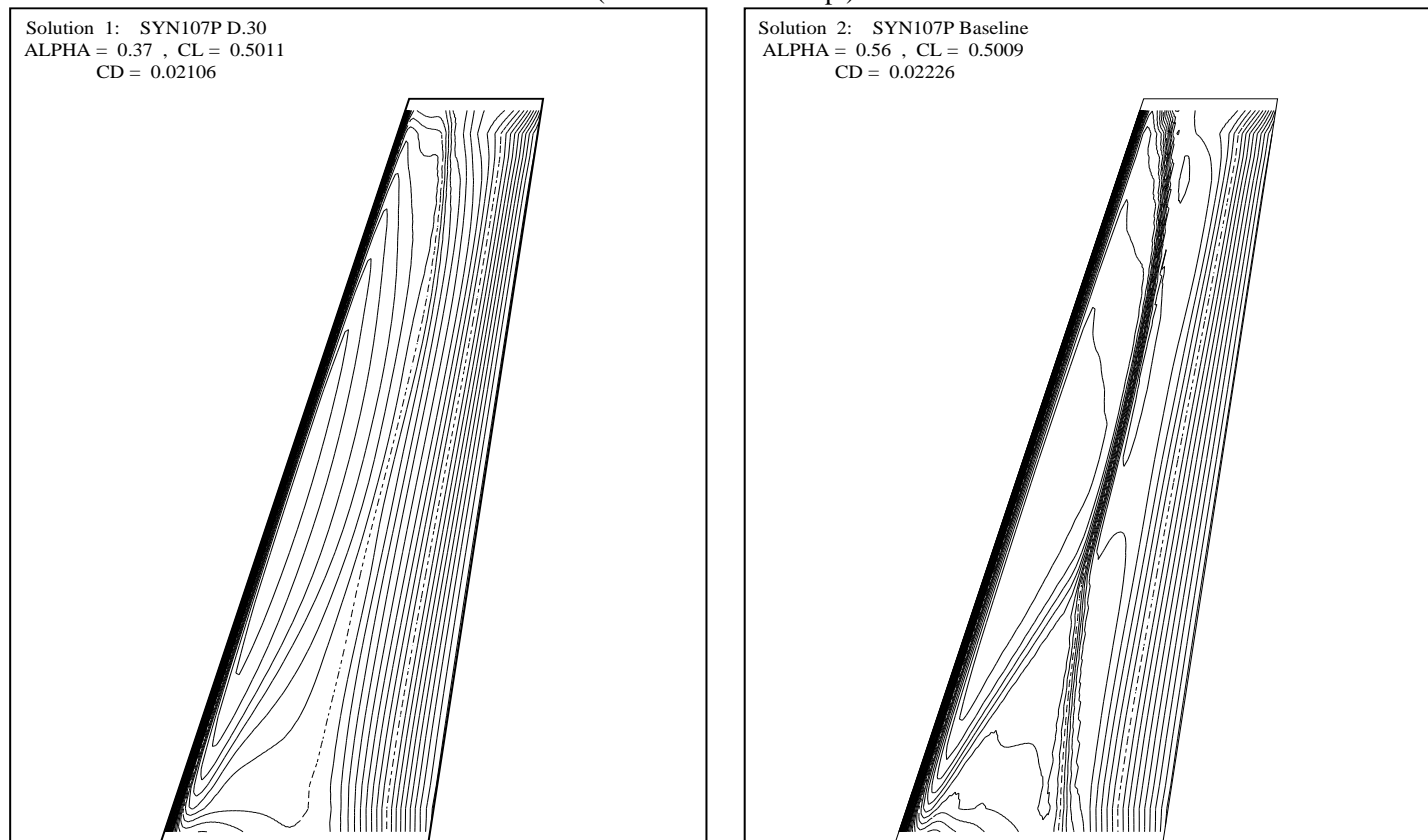


Figure 4. SYN107. One-point optimization Case-S1. Upper surface C_p countours at $M = 0.76$, $C_L = 0.50$.

COMPLOT
Ver 2.01



John C. Vassberg
17:33 Fri
25 May 07

COMPARISON OF LOWER SURFACE CONTOURS DPW-W1 WING (FLAT TIP AT Y=762.0)

REN = 5.00 , MACH = 0.760

(Contours at 0.05 Cp)

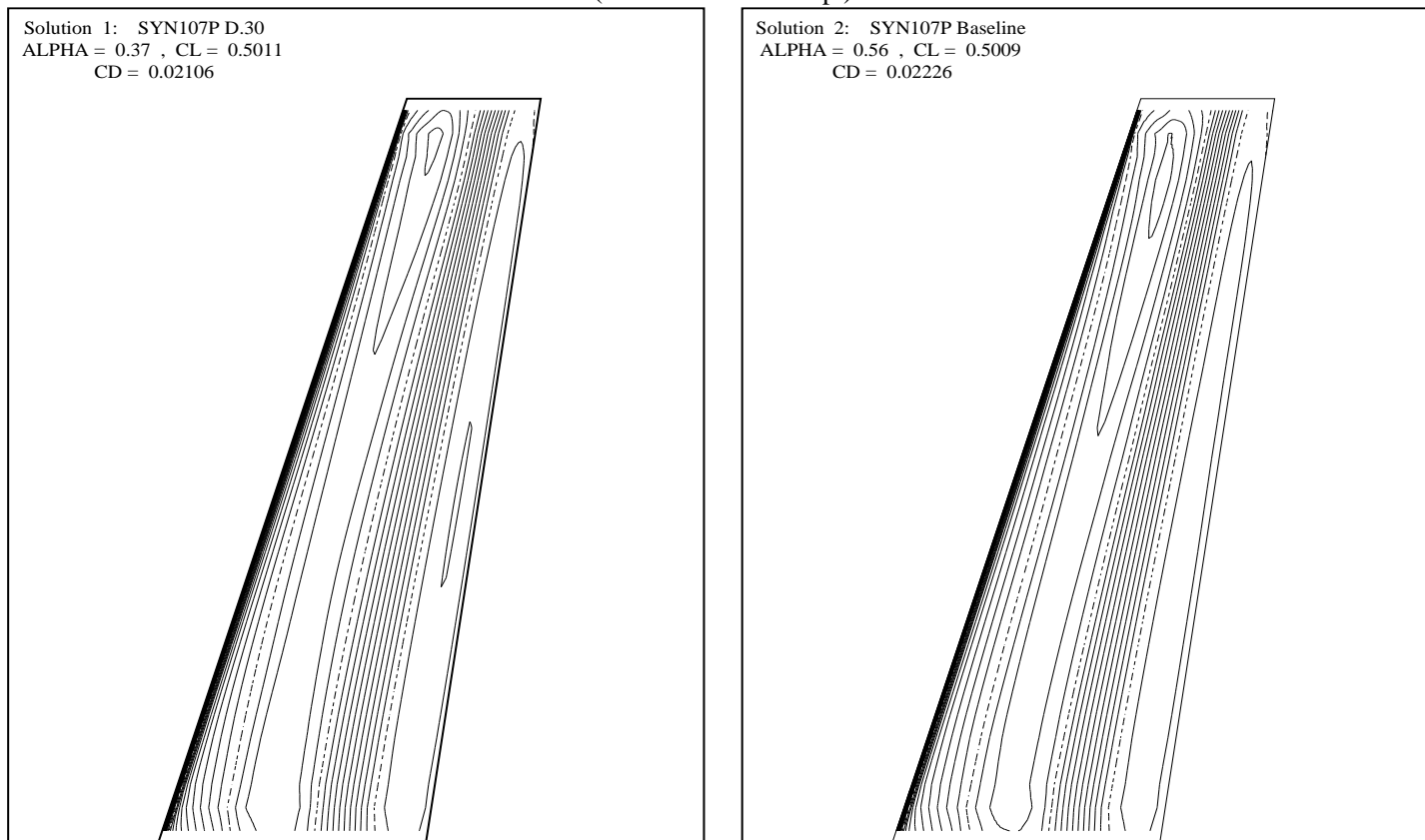


Figure 5. SYN107. One-point optimization Case_S1. Lower surface C_p countours at $M = 0.76$, $C_L = 0.50$.

COMPLOT
Ver 2.01



John C. Vassberg
17:33 Fri
25 May 07

COMPARISON OF CHORDWISE PRESSURE DISTRIBUTIONS IAI-W1-76-77-78-50

REN = 5.0

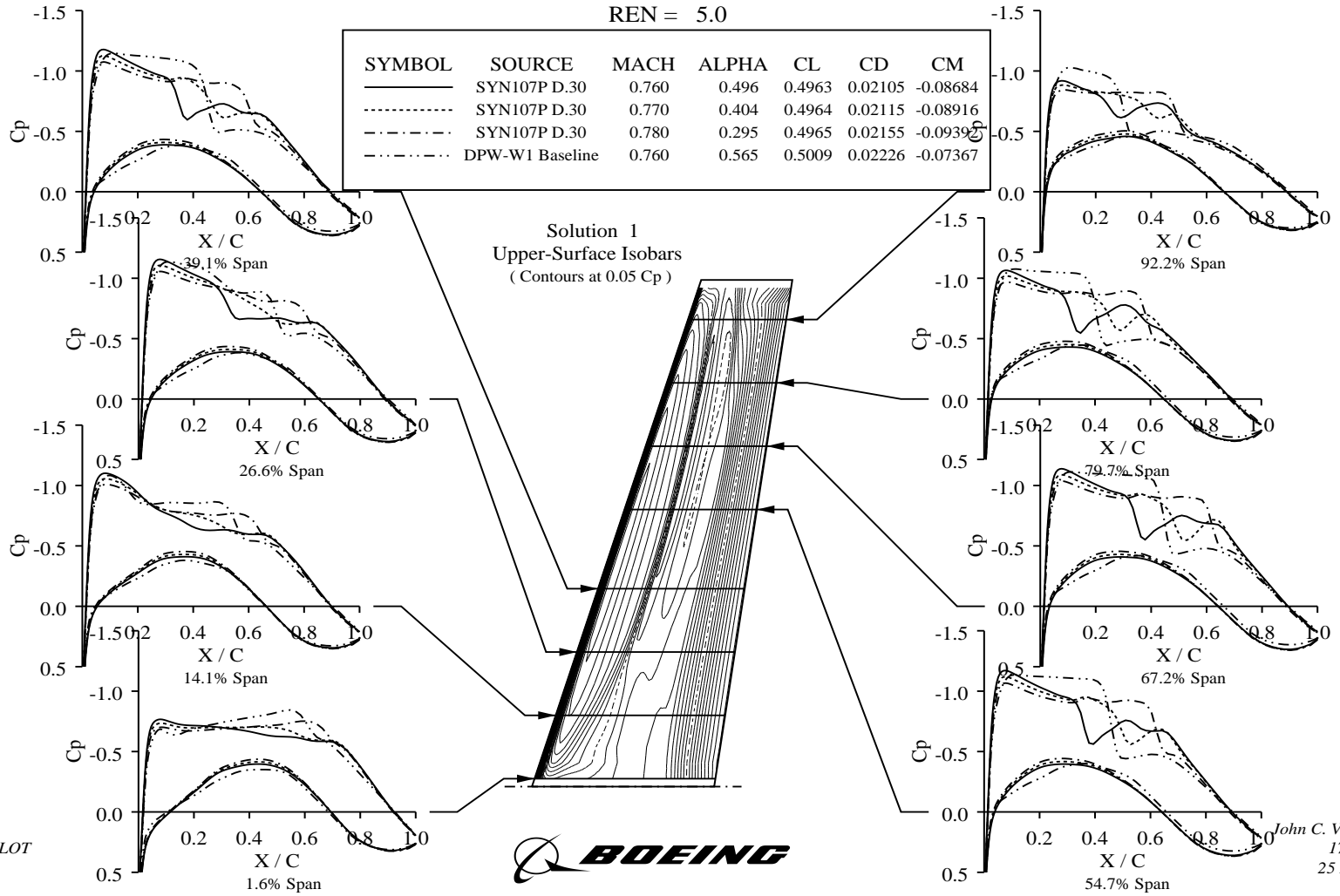


Figure 6. SYN107. Three-point optimization Case-53. Chordwise pressure distributions at $M = 0.76 - 0.78$, $C_L = 0.50$.

COMPPLOT
Ver 2.01

John C. Vassberg
17:54 Fri
25 May 07

COMPARISON OF UPPER SURFACE CONTOURS IAI-W1-78-50

REN = 5.0

(Contours at 0.05 Cp)

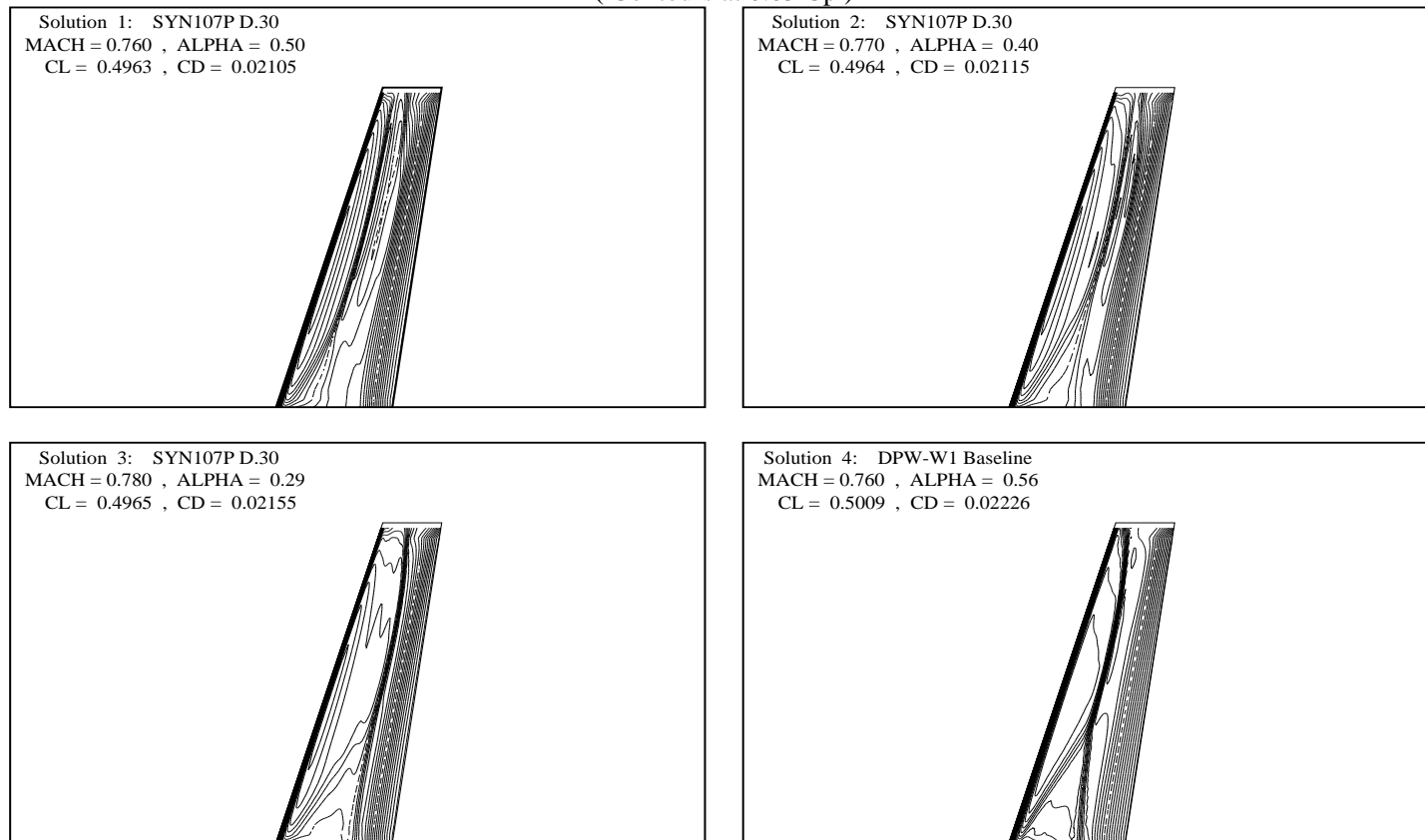


Figure 7. SYN107. Three-point optimization Case-S3. Upper surface Cp contours at $M = 0.76 - 0.78$, $C_L = 0.50$.

COMPARISON OF LOWER SURFACE CONTOURS IAI-W1-78-50

REN = 5.0

(Contours at 0.05 Cp)

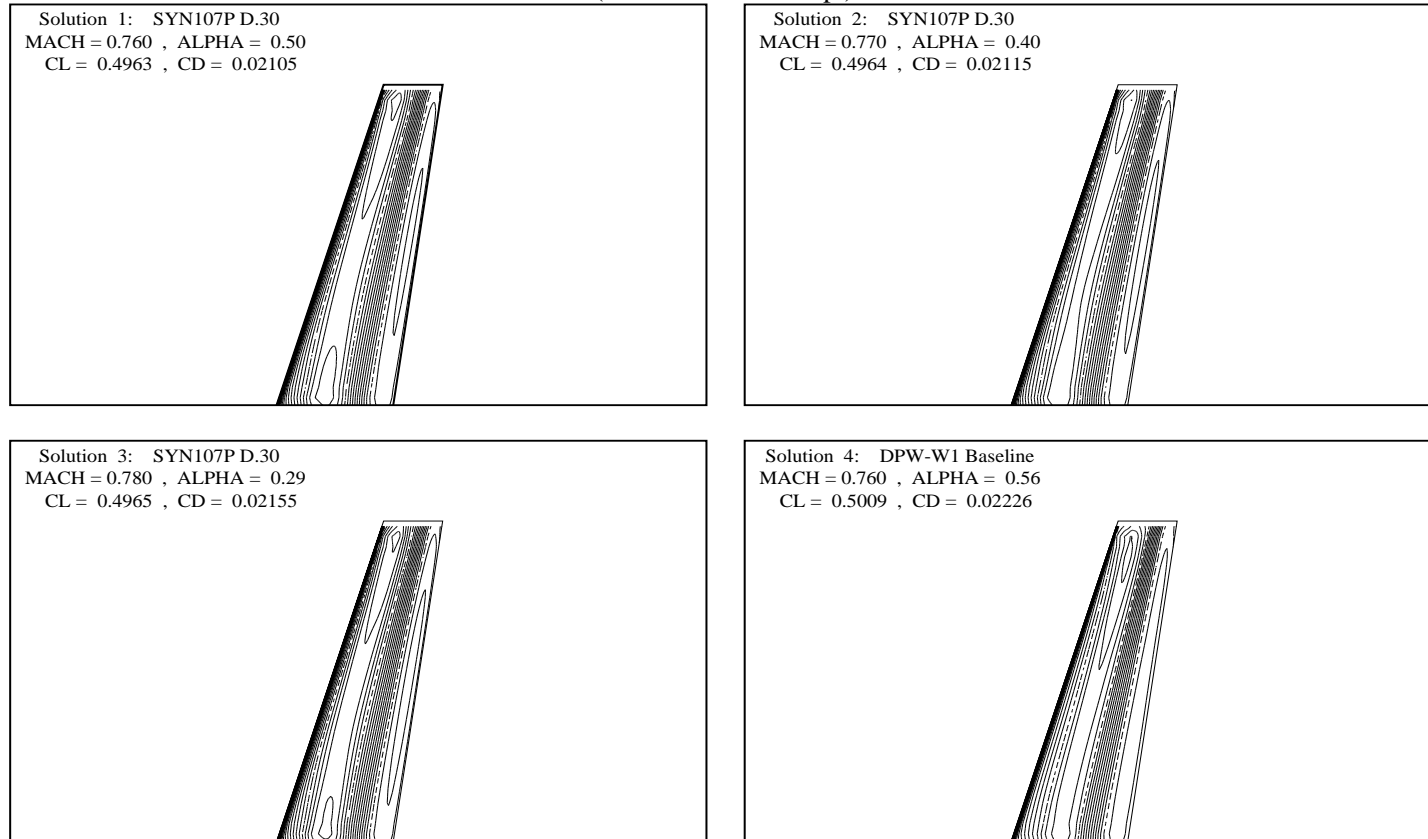


Figure 8. SYN107. Three-point optimization Case-S3. Lower surface Cp countours at $M = 0.76 - 0.78$, $C_L = 0.50$.

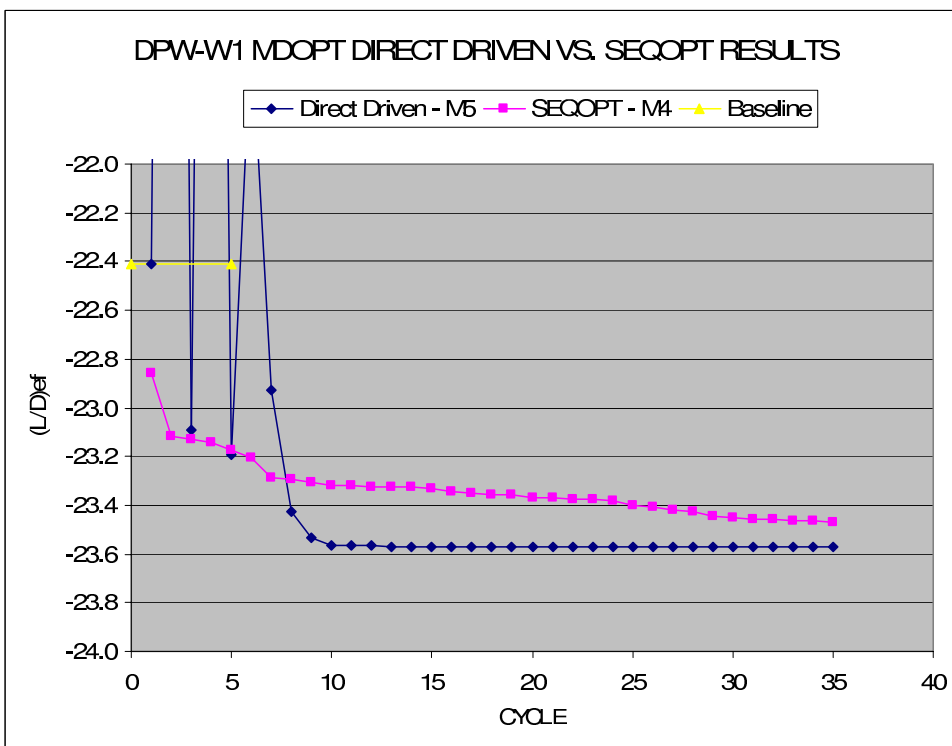


Figure 9. MDOPT. Direct Driven vs. SEQOPT results.

COMPARISON OF SPANLOAD DISTRIBUTIONS
 DPW-W1 MDOPT/TLNS
 REN = 5M , MACH = 0.760

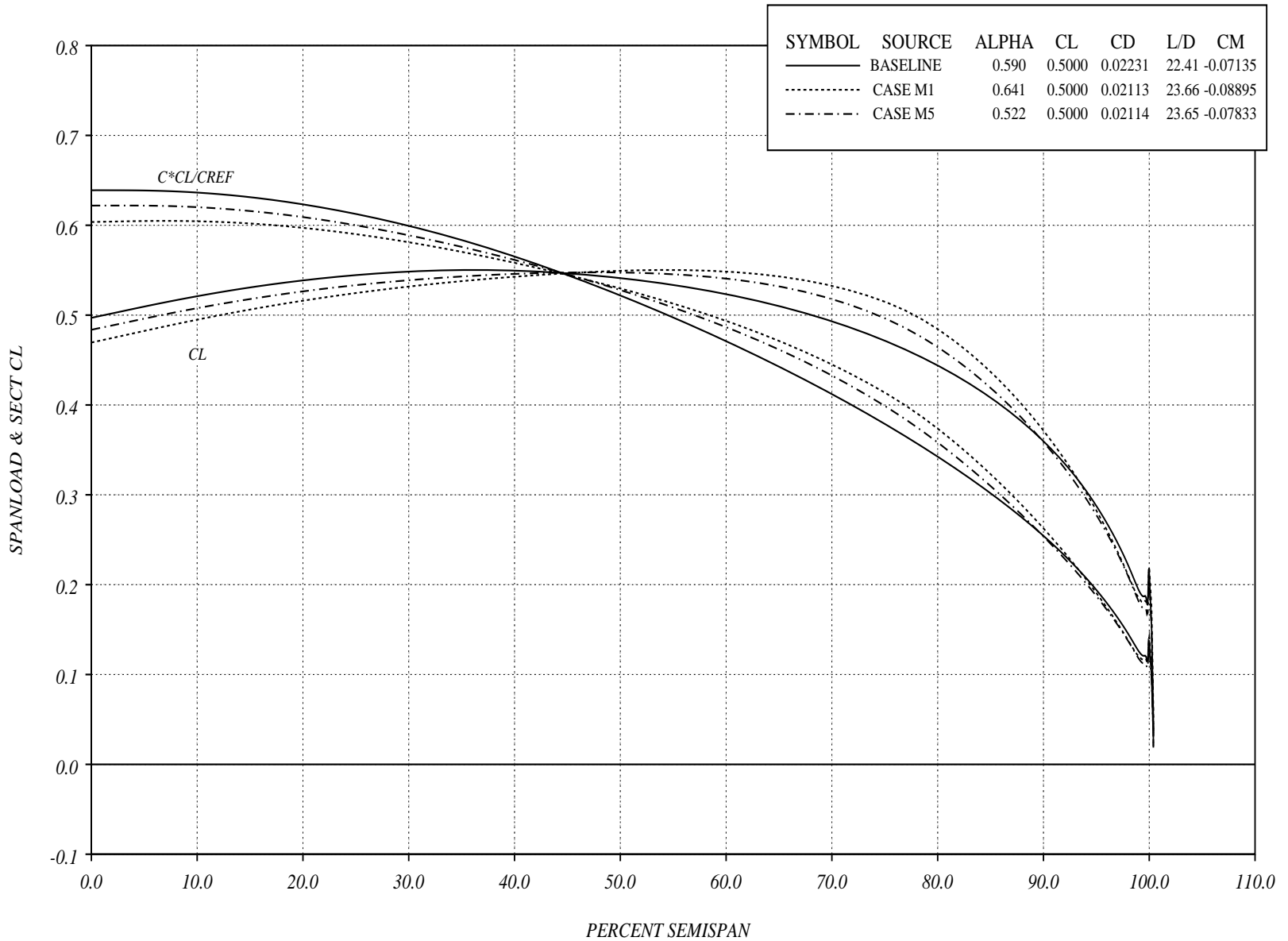


Figure 10. MDOPT. Comparison of spanload distributions for Case_M1 and Case_M5 at $M = 0.76$.

COMPARISON OF CHORDWISE PRESSURE DISTRIBUTIONS
 DPW-W1 MDOPT/TLNS
 REN = 5M, MACH = 0.760

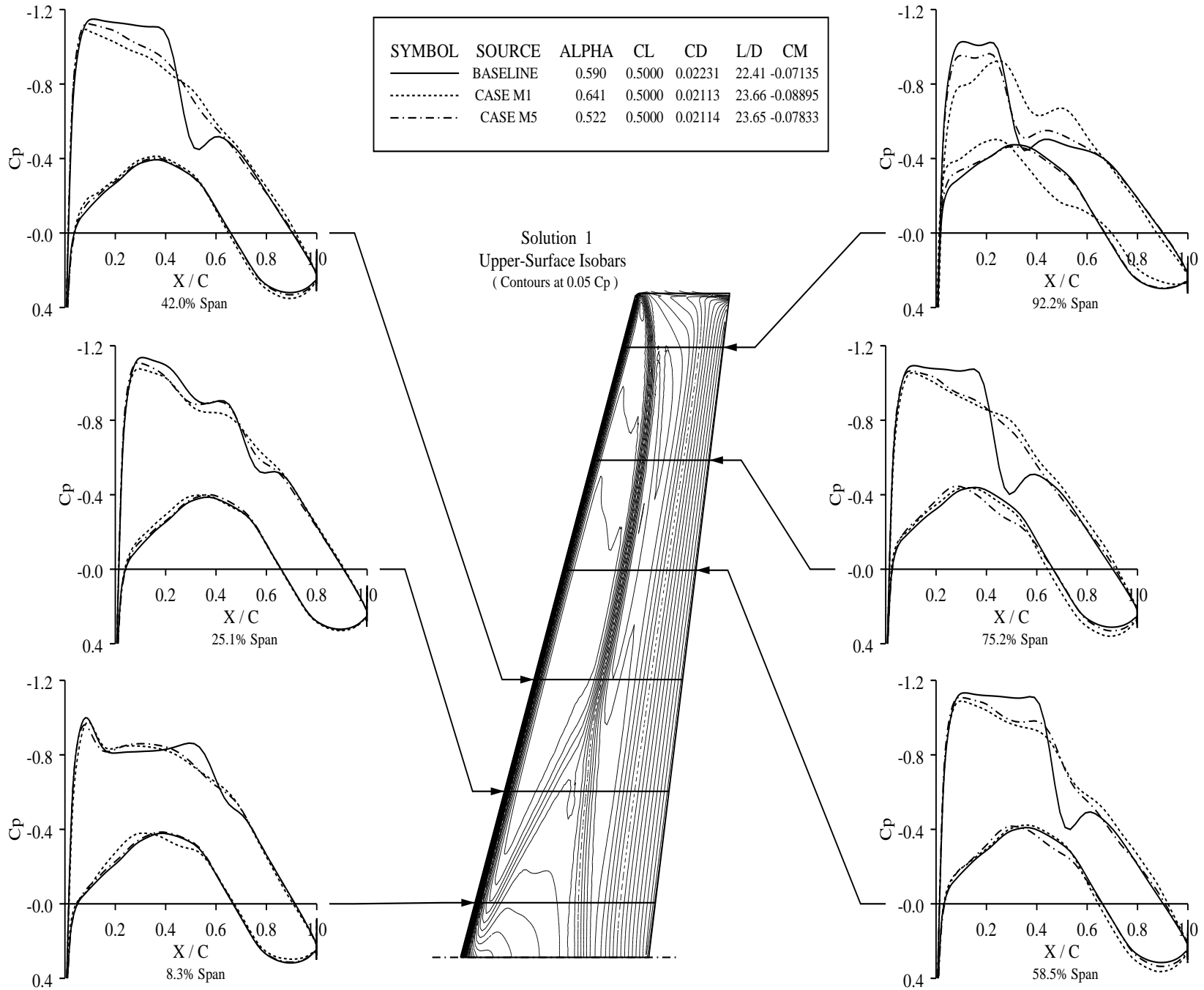


Figure 11. MDOPT. Comparison of chordwise pressure distributions for Case-M1 and Case-M5 at $M = 0.76$.

COMPARISON OF CHORDWISE PRESSURE DISTRIBUTIONS DPW-W1 MDOPT/TLNS

REN = 5M , MACH = 0.760

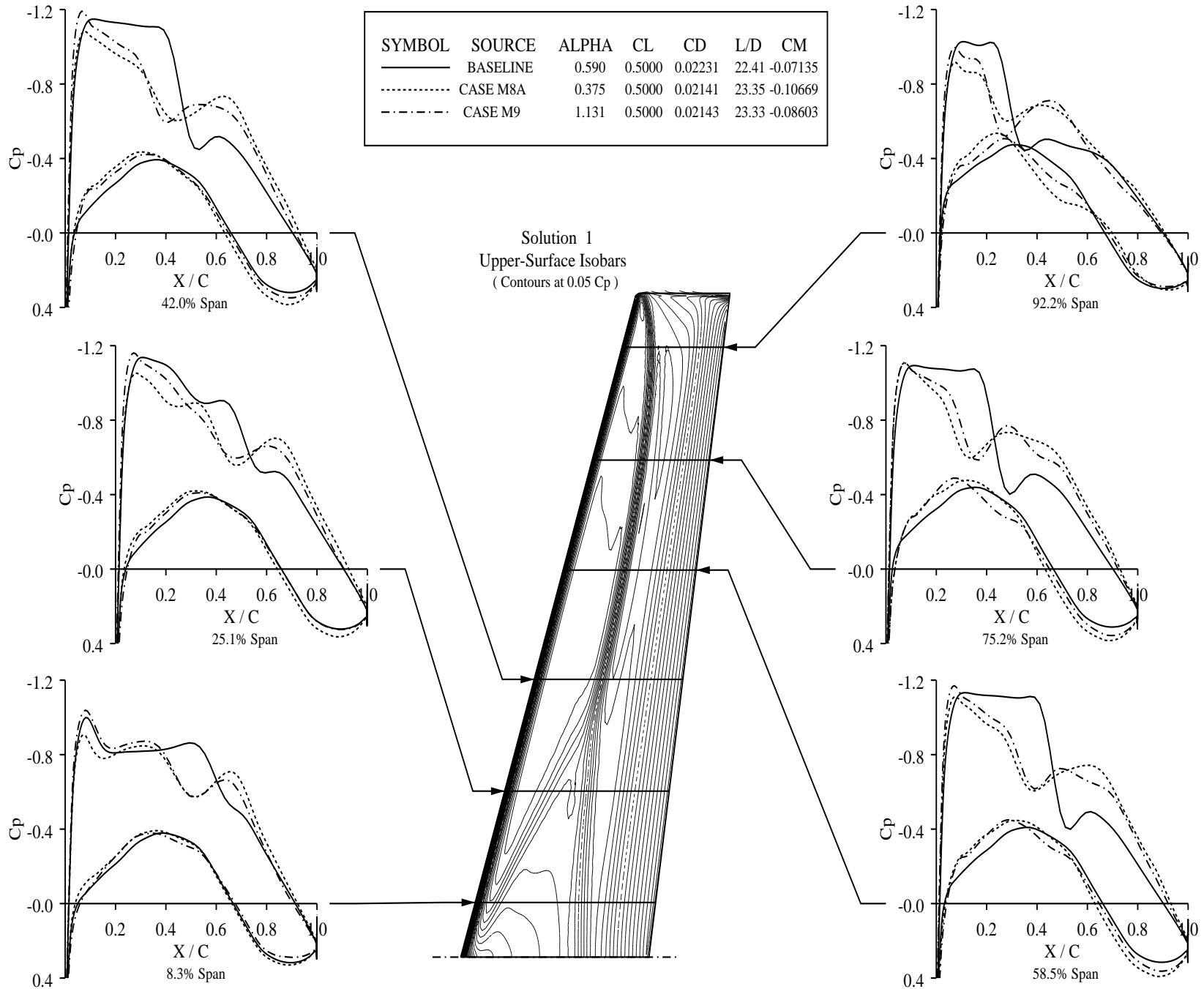


Figure 12. MDOPT. Comparison of chordwise pressure distributions for the dual-point optimization cases at $M = 0.76$.

COMPARISON OF CHORDWISE PRESSURE DISTRIBUTIONS DPW-W1 MDOPT/TLNS REN = 5M , MACH = 0.780

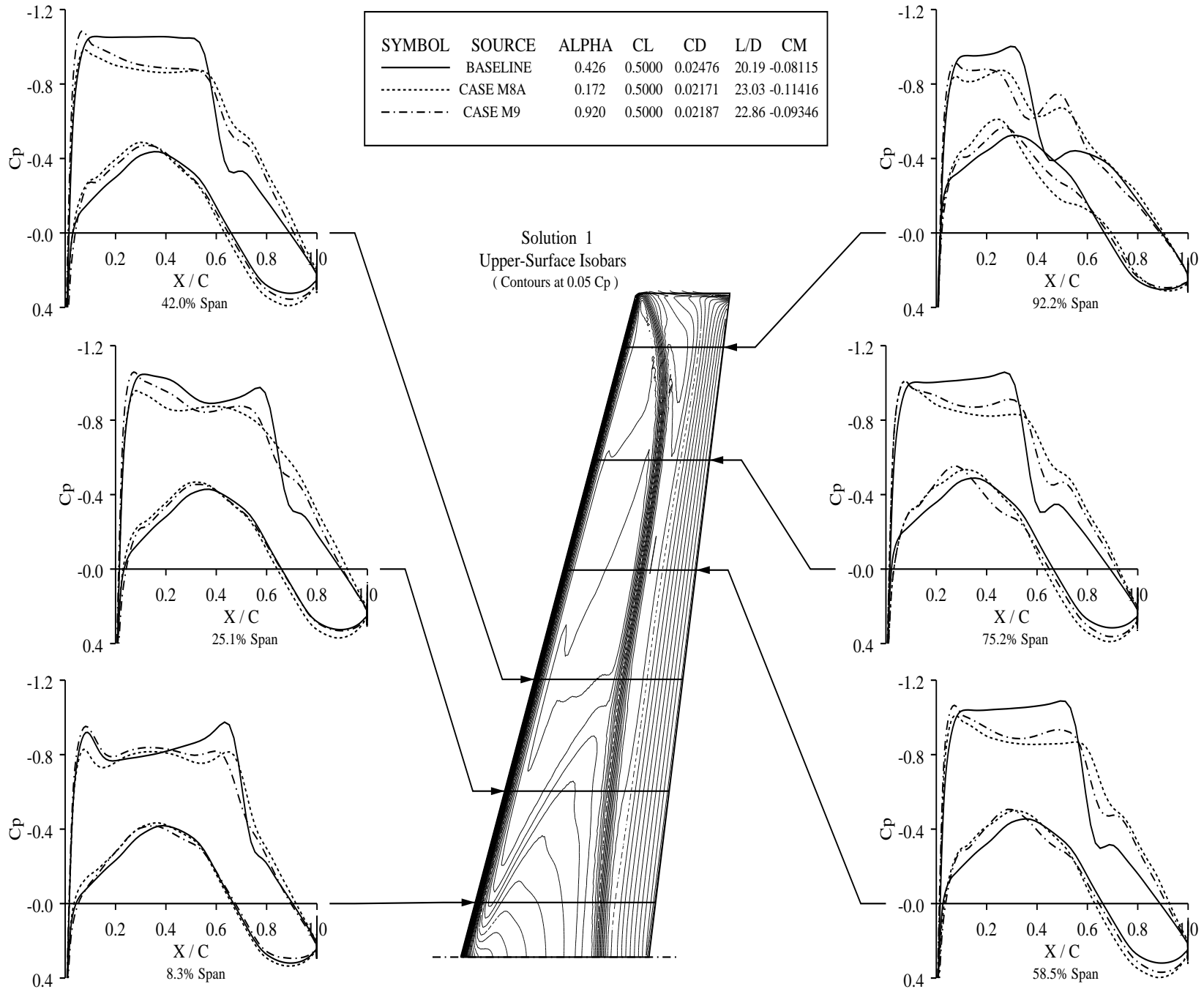


Figure 13. MDOPT. Comparison of chordwise pressure distributions for the dual-point optimization cases at $M = 0.78$.

COMPARISON OF SPANLOAD DISTRIBUTIONS
 DPW-W1 MDOPT/TLNS
 REN = 5M , MACH = 0.760

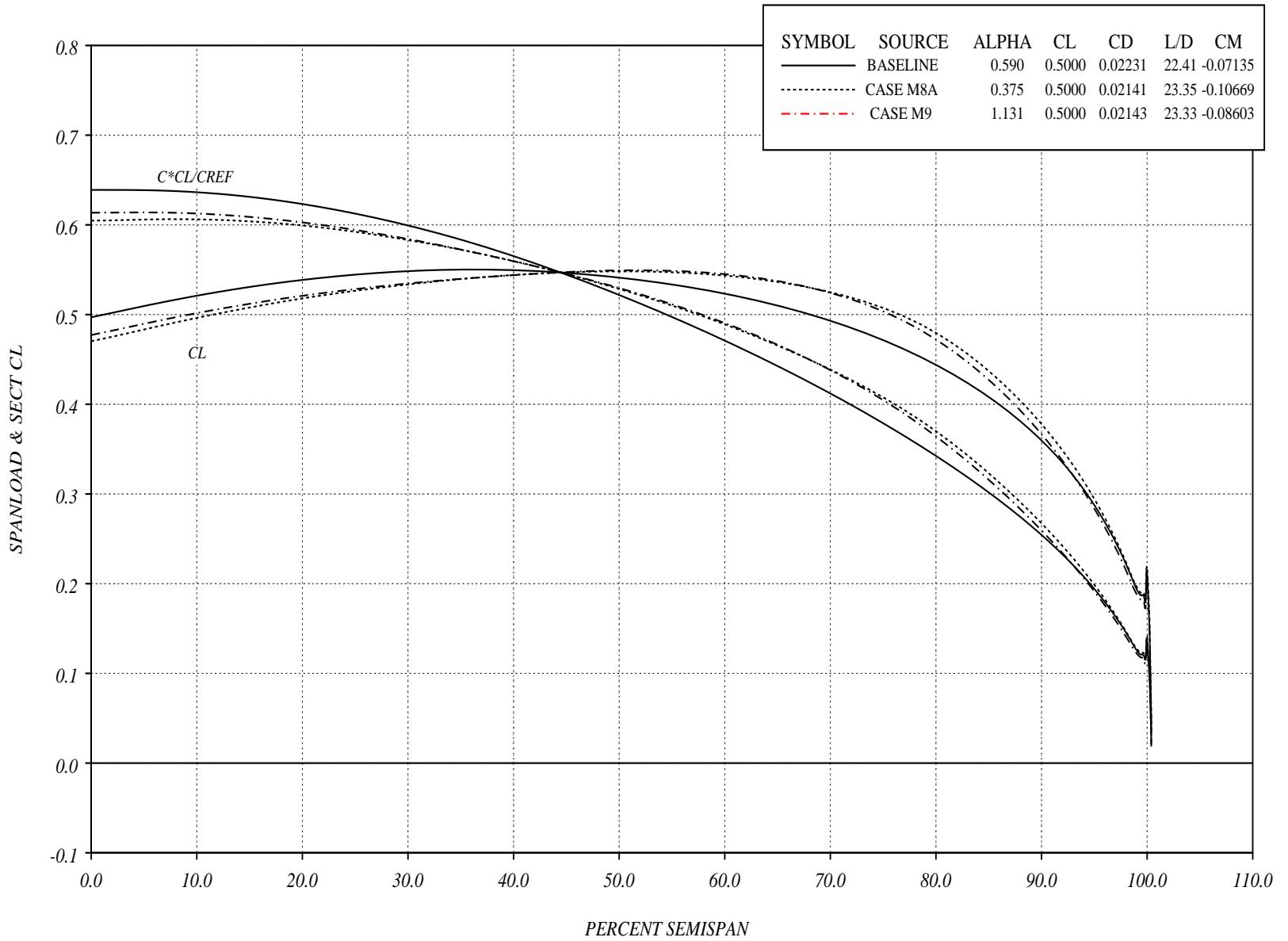


Figure 14. MDOPT. Comparison of spanload distributions for the dual-point optimization cases at $M = 0.76$.



COMPARISON OF SPANLOAD DISTRIBUTIONS
 DPW-W1 MDOPT/TLNS
 REN = 5M , MACH = 0.780

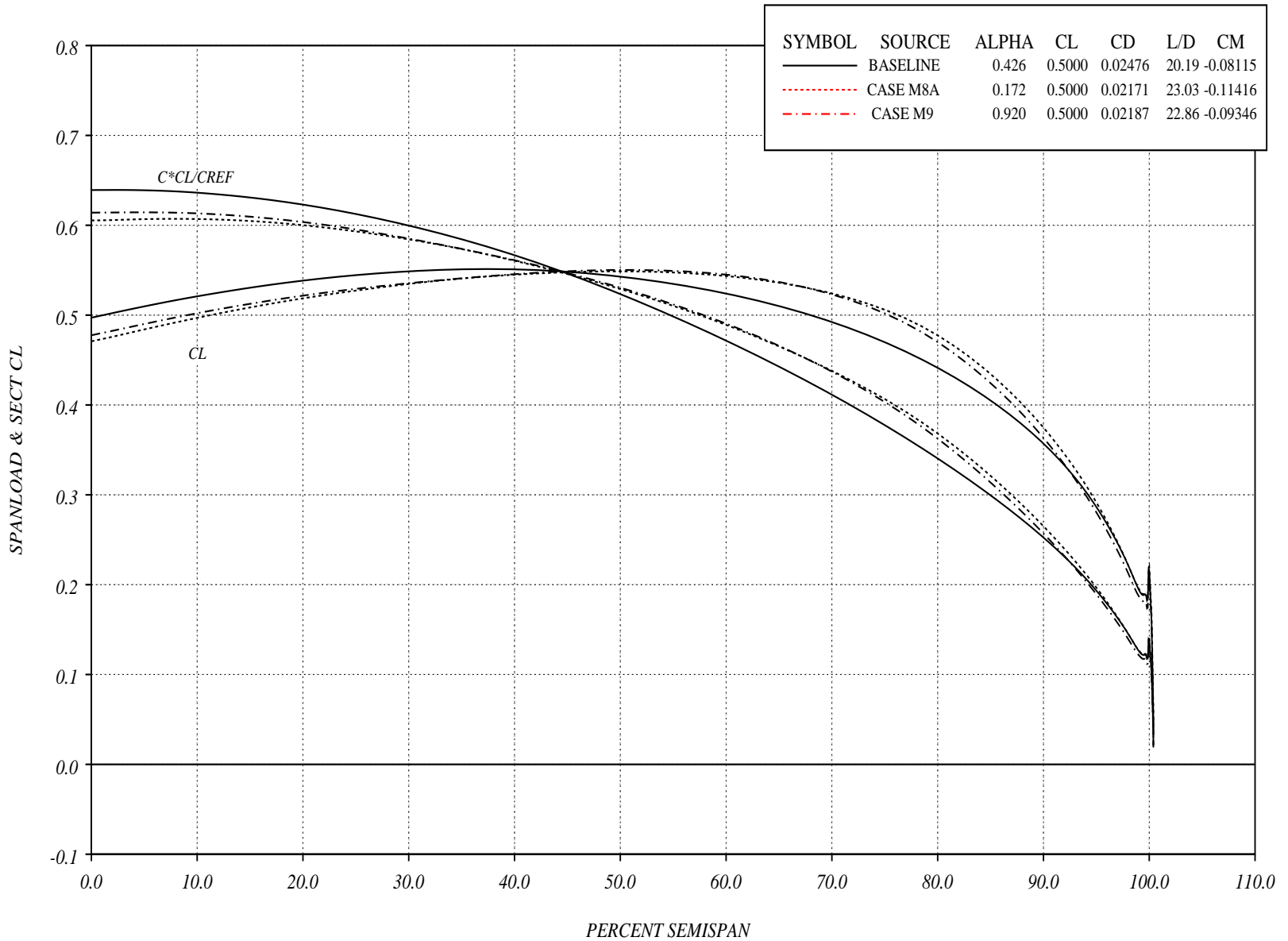


Figure 15. MDOPT. Comparison of spanload distributions for the dual-point optimization cases at $M = 0.78$.

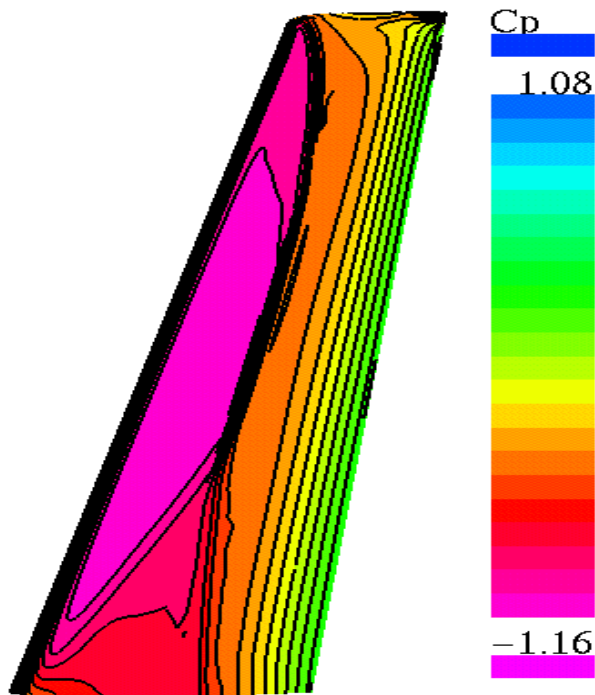


Figure 16. Pressure distribution on the upper surface of the original wing at $M = 0.76$, $C_L = 0.50$.

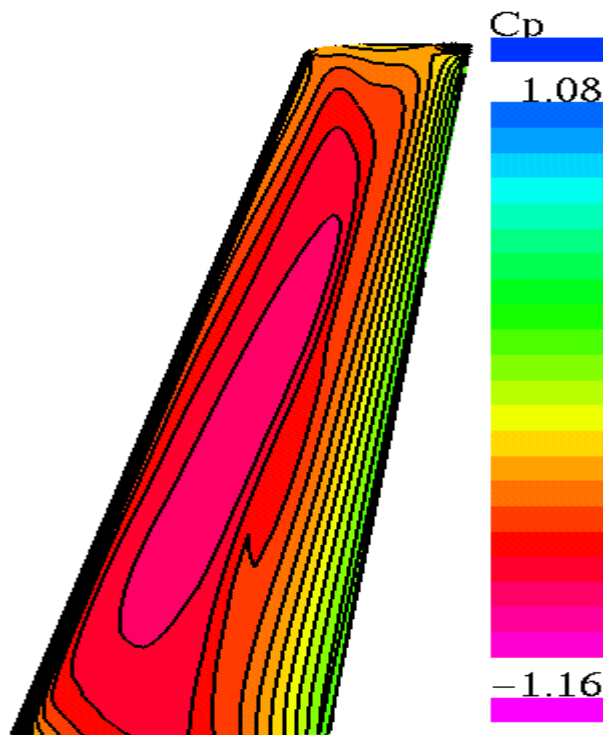


Figure 17. Pressure distribution on the upper surface of the optimal wing. *Case_O1* at $M = 0.76$, $C_L = 0.50$.

DPW-W1 wing alone. Drag Polars at M=0.76

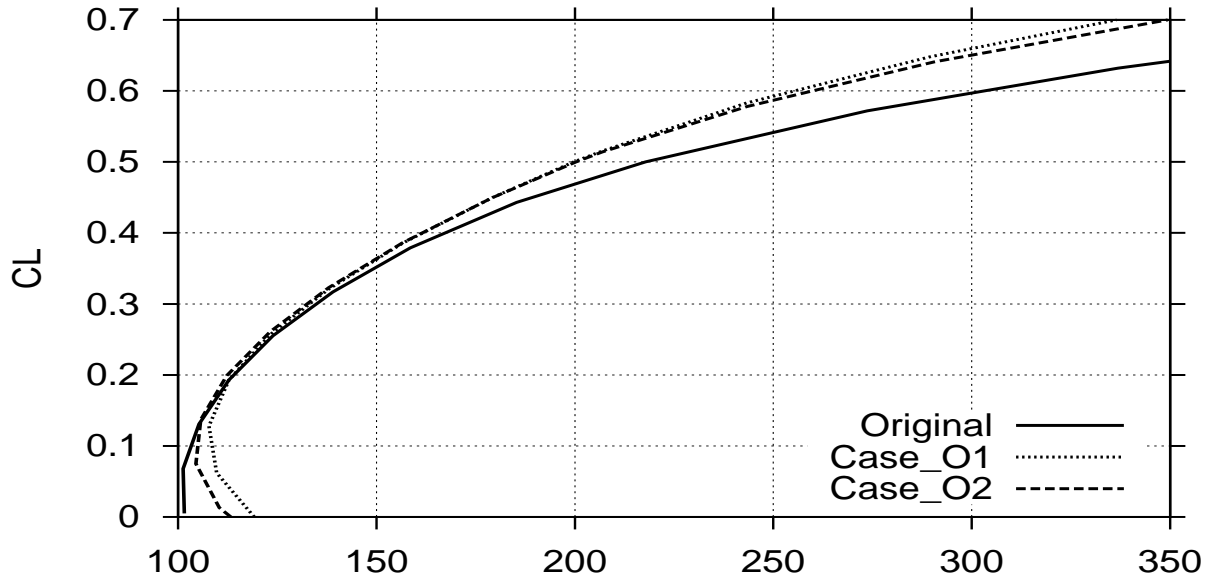


Figure 18. Lift/drag polars at $M = 0.76$, $Re = 5.0 \cdot 10^6$. Original wing vs optimized ones.

DPW-W1 wing alone. Drag Divergence at $CL=0.5$

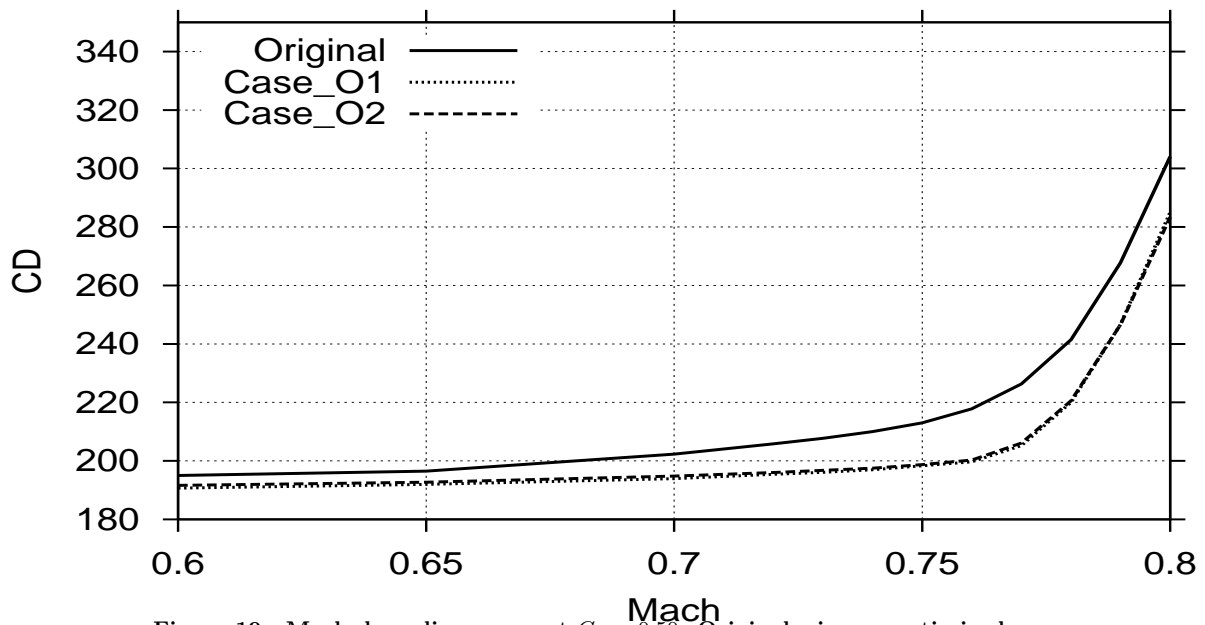


Figure 19. Mach drag divergence at $C_L = 0.50$. Original wing vs optimized ones.

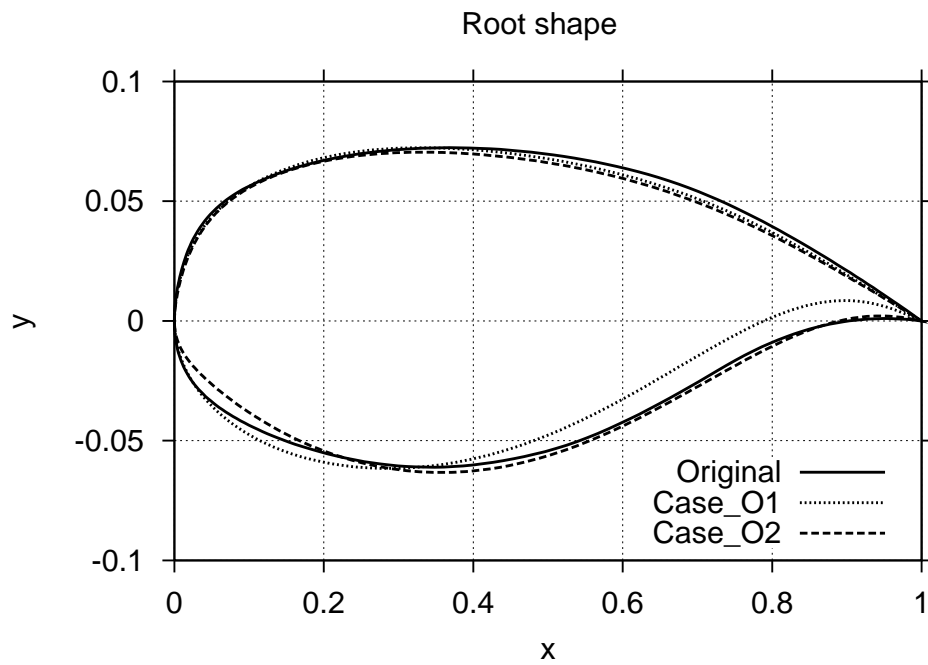


Figure 20. Root wing section. Original vs optimized ones.

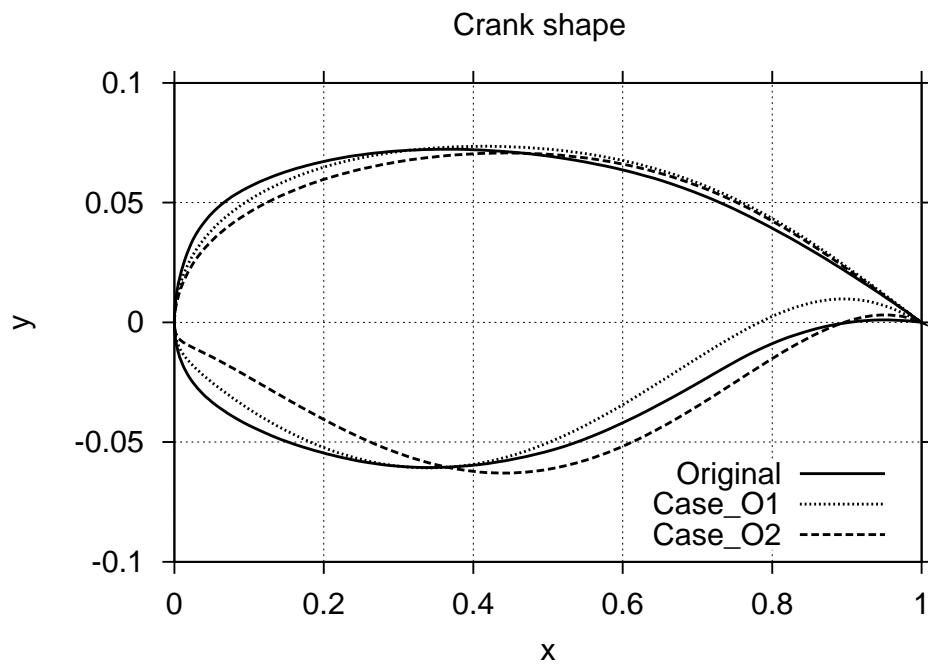


Figure 21. Crank wing section at $2Y/b = 0.375$. Original vs optimized ones.

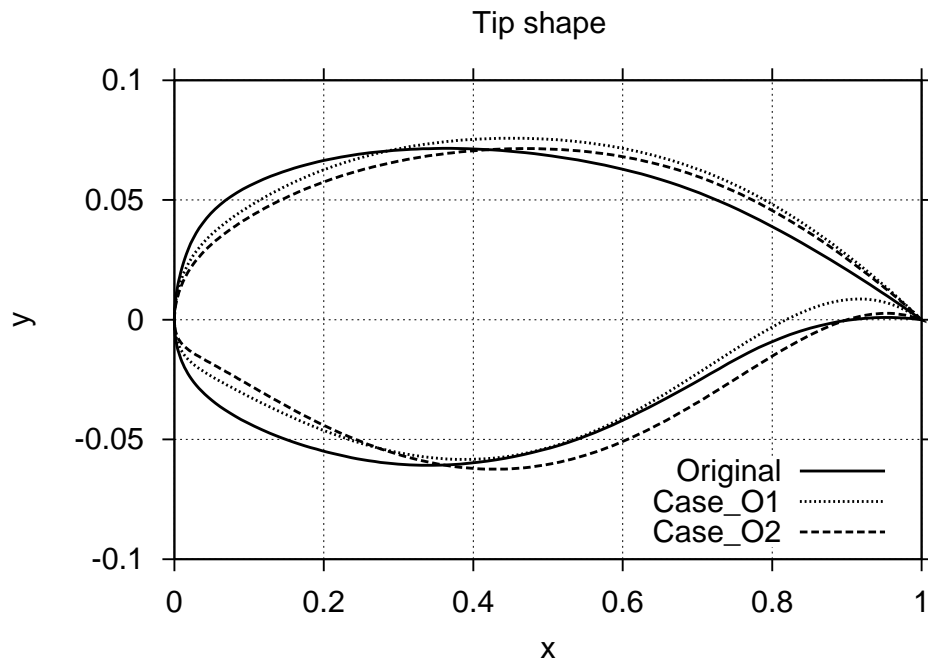


Figure 22. Tip wing section. Original vs optimized ones.

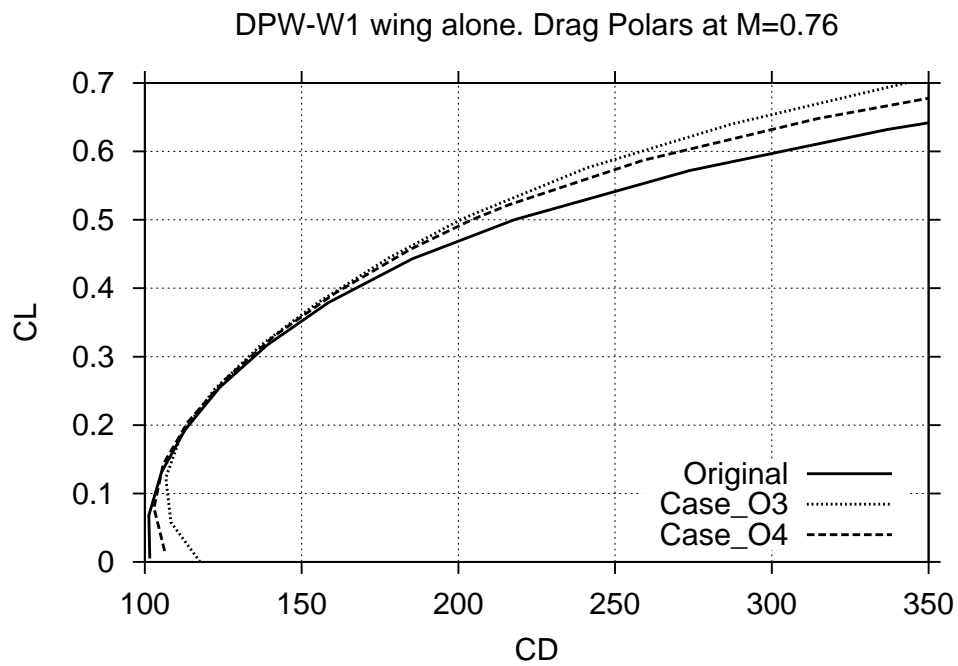


Figure 23. Lift/drag polars at $M = 0.76$, $Re = 5.0 \cdot 10^6$. Original wing vs optimized ones.

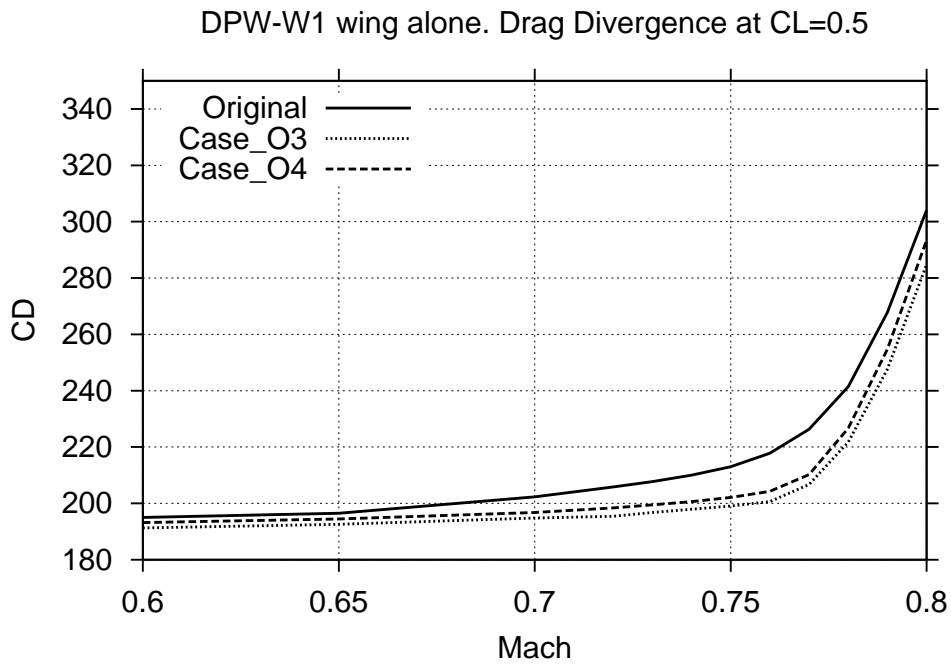


Figure 24. Mach drag divergence at $C_L = 0.50$. Original wing vs optimized ones.

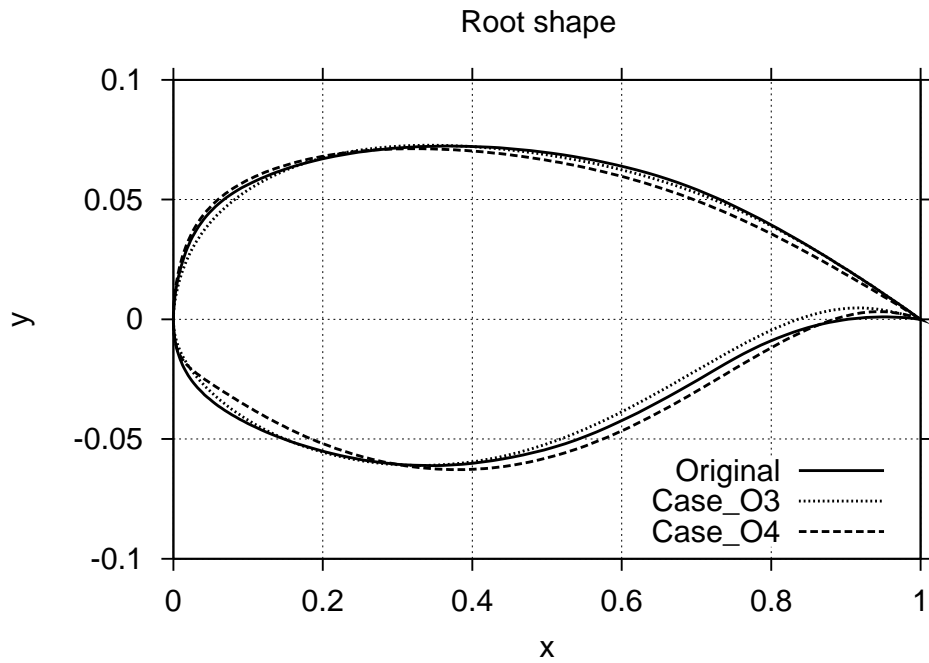


Figure 25. Root wing section. Original vs optimized ones.

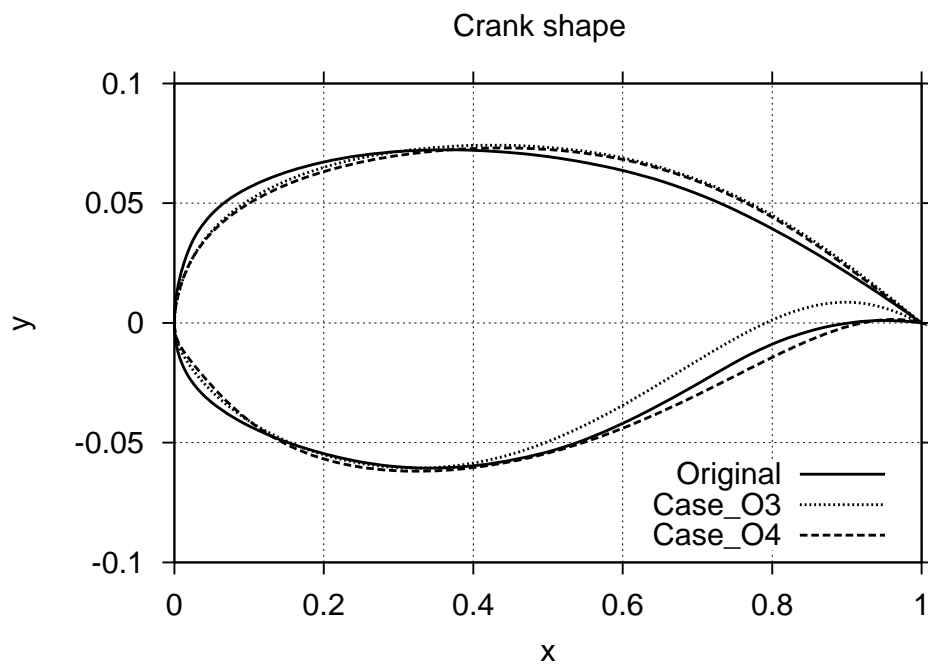


Figure 26. Crank wing section at $2Y/b = 0.375$. Original vs optimized ones.

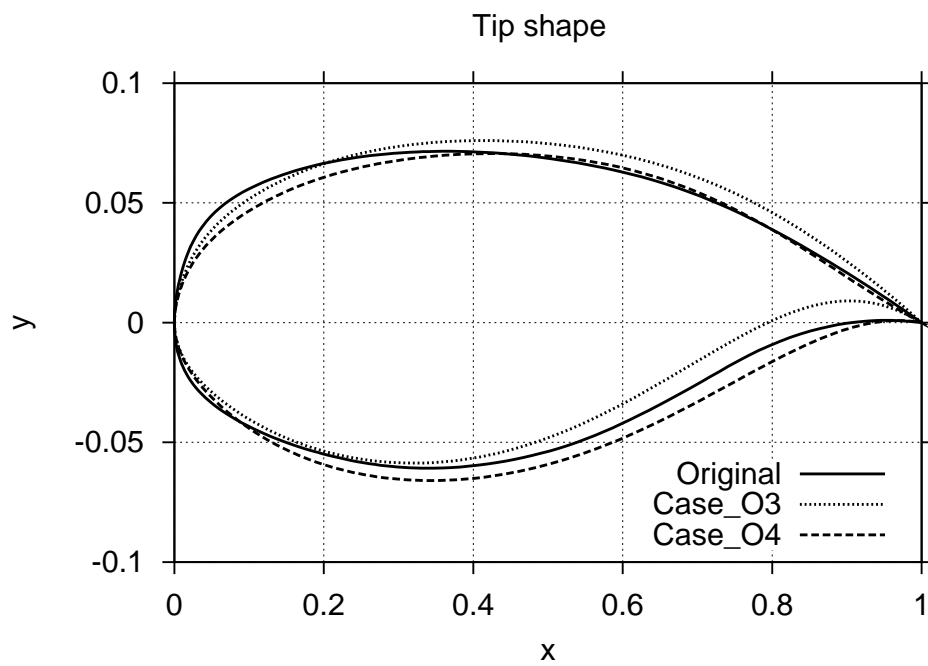


Figure 27. Tip wing section. Original vs optimized ones.

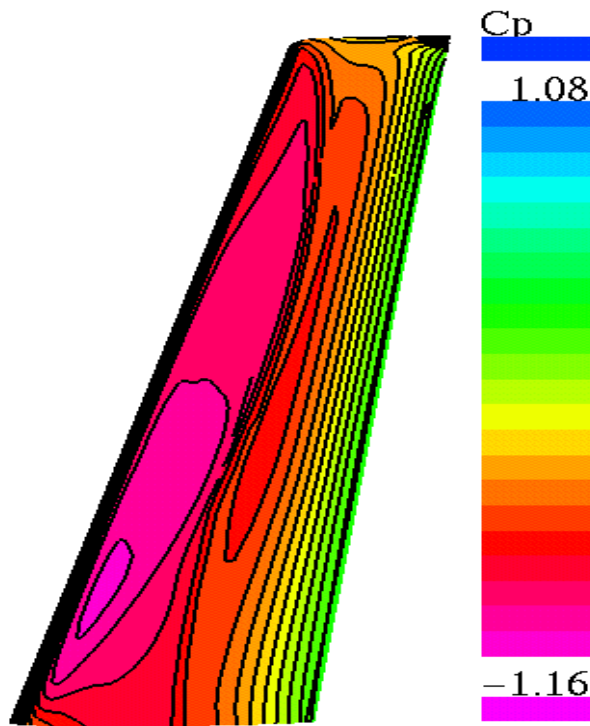


Figure 28. Pressure distribution on the upper surface of the optimal wing. *Case_O5* at $M = 0.76$, $C_L = 0.50$.

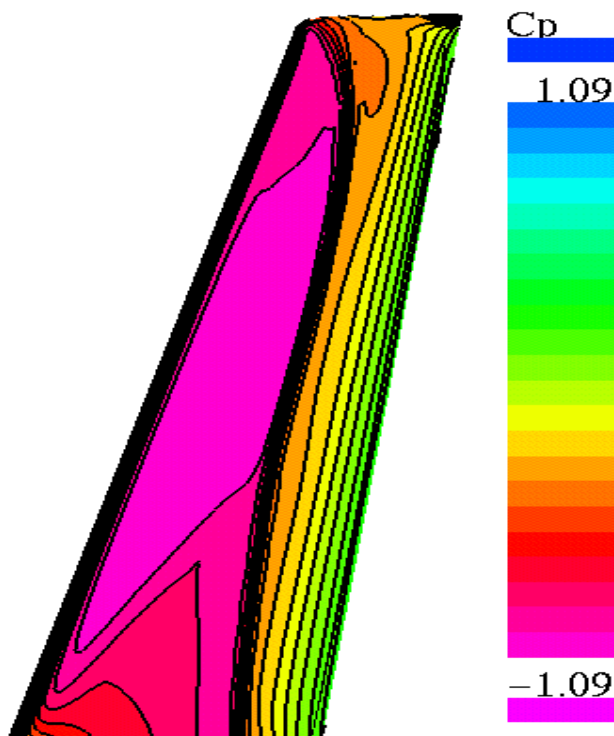


Figure 29. Pressure distribution on the upper surface of the original wing. $M = 0.78$, $C_L = 0.50$.

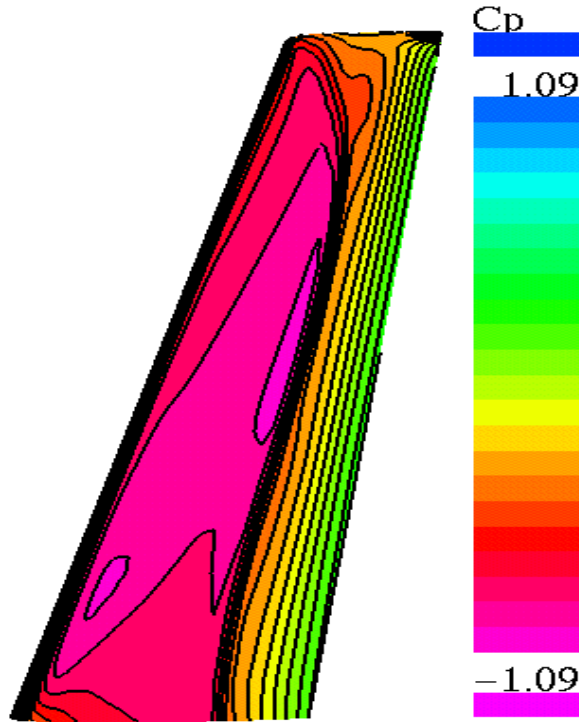


Figure 30. Pressure distribution on the upper surface of the optimal wing. *Case_O5* at $M = 0.78$, $C_L = 0.50$.

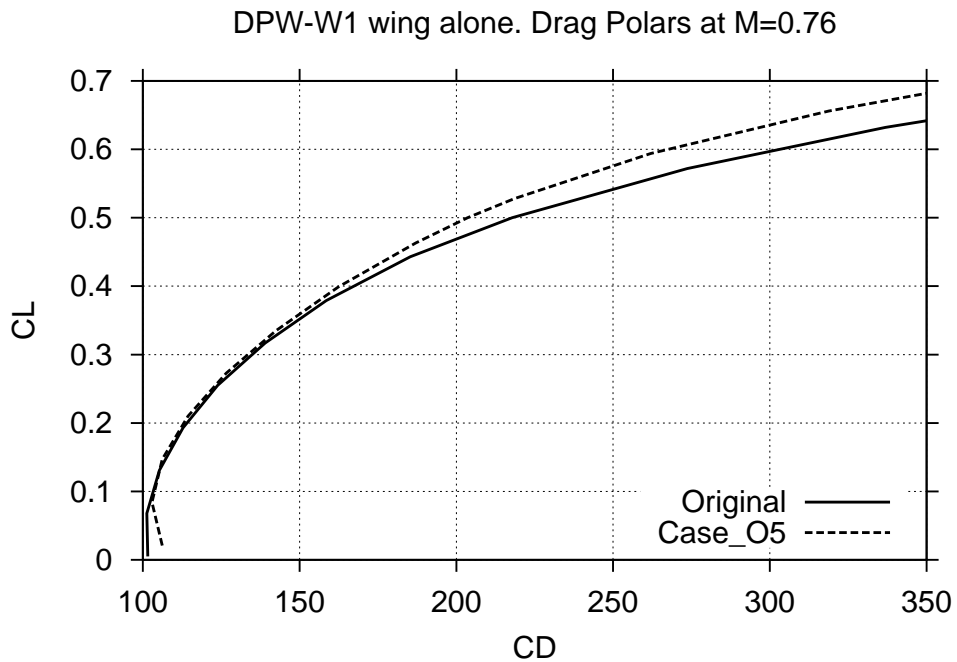


Figure 31. Lift/drag polars at $M = 0.76$, $Re = 5.0 \cdot 10^6$. Original wing vs optimized one.

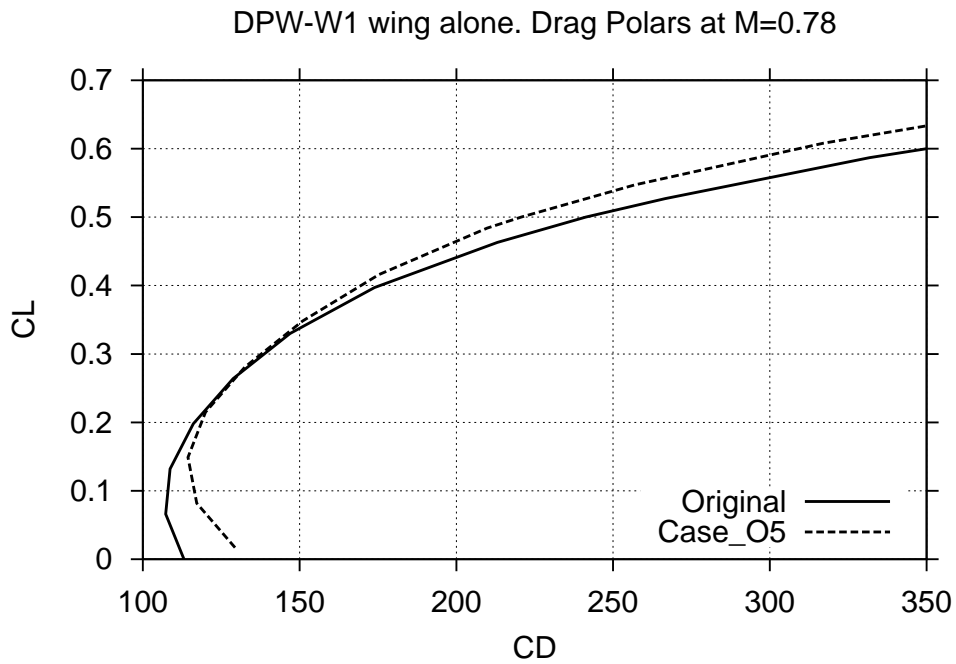


Figure 32. Lift/drag polars at $M = 0.78$, $Re = 5.0 \cdot 10^6$. Original wing vs optimized one.

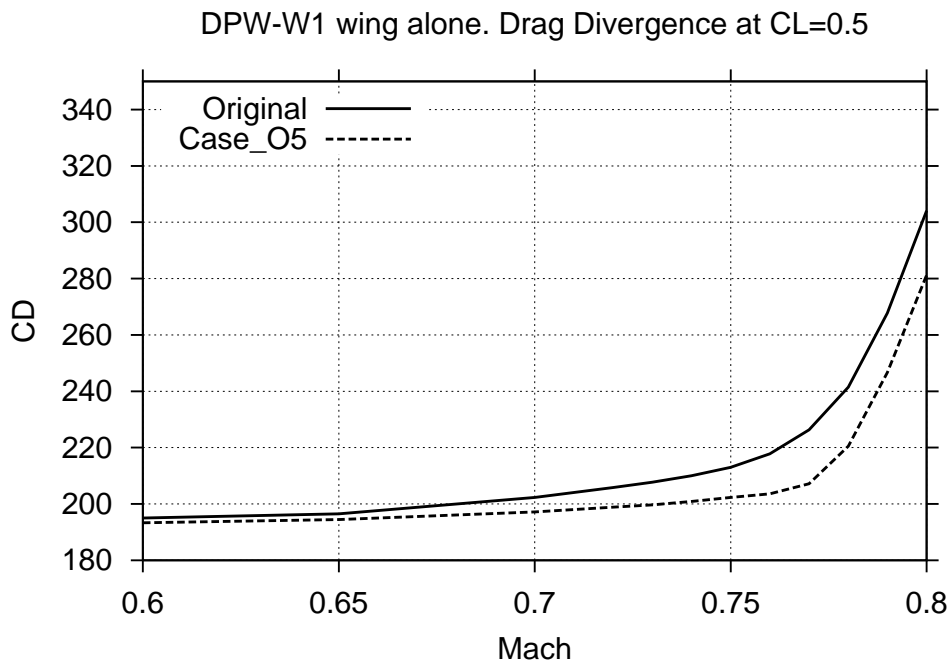


Figure 33. Mach drag divergence at $C_L = 0.50$. Original wing vs optimized one.

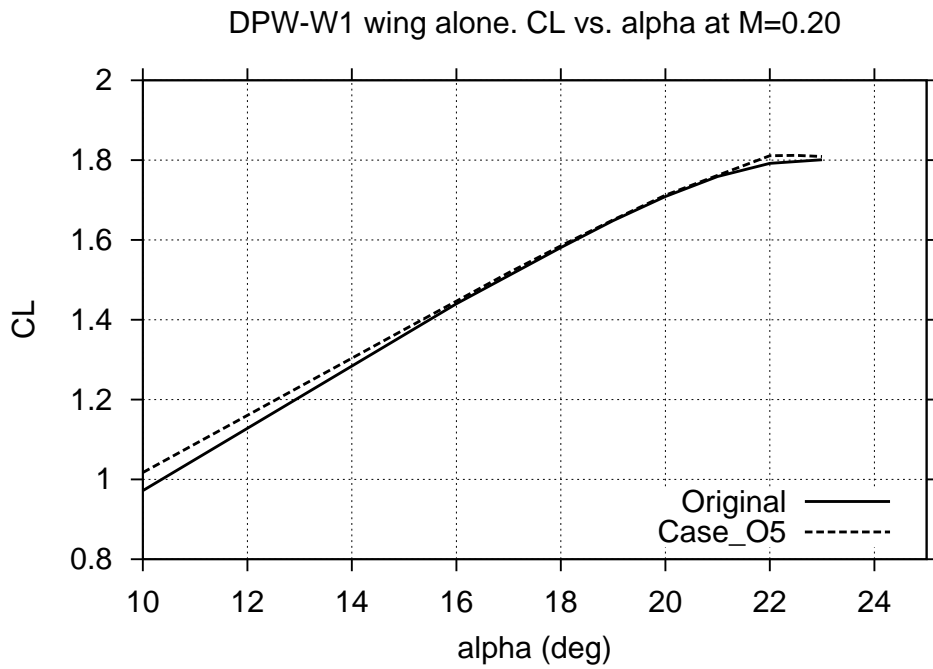


Figure 34. C_L vs. angle of attack at take-off conditions. Original wing vs optimized one.

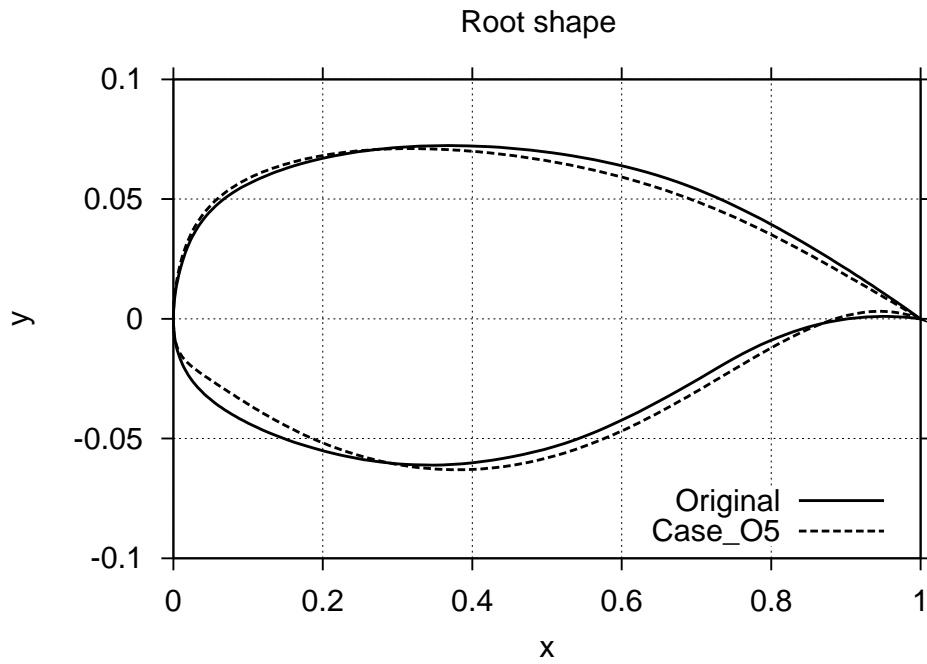


Figure 35. Root wing section. Original vs optimized ones.

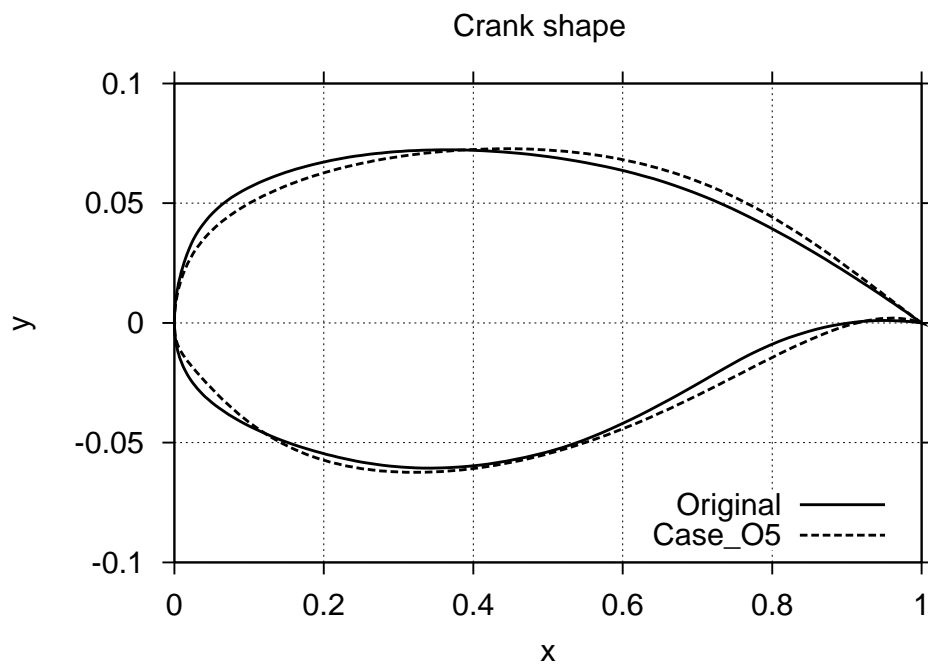


Figure 36. Crank wing section at $2Y/b = 0.375$. Original vs optimized ones.

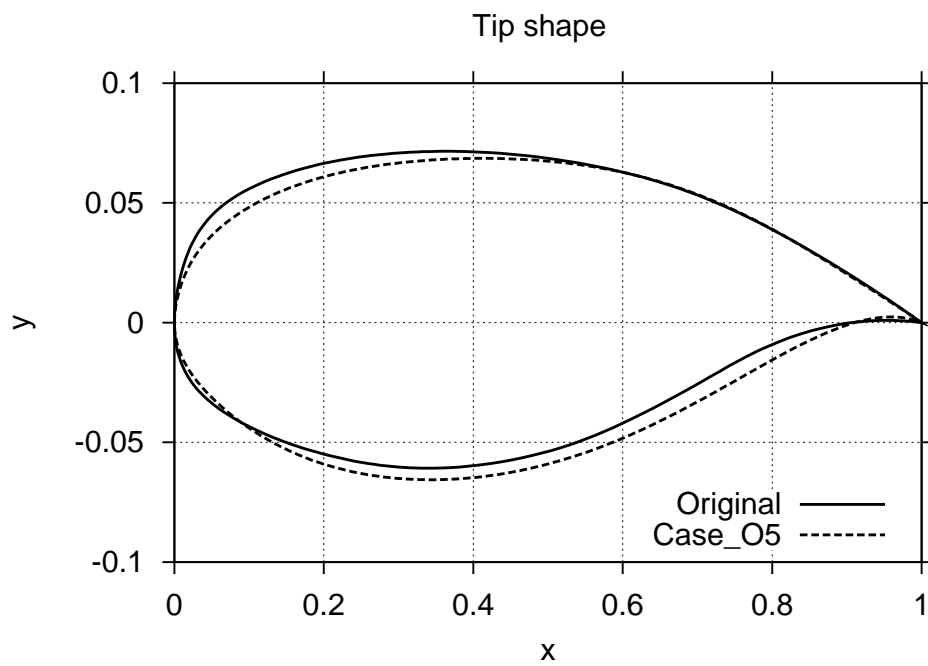


Figure 37. Tip wing section. Original vs optimized ones.

COMPARISON OF CHORDWISE PRESSURE DISTRIBUTIONS SINGLE-POINT OPTIMIZATIONS OF DPW-W1 WING OVERFLOW , MACH = 0.760 , CL = 0.500 , REN=5M

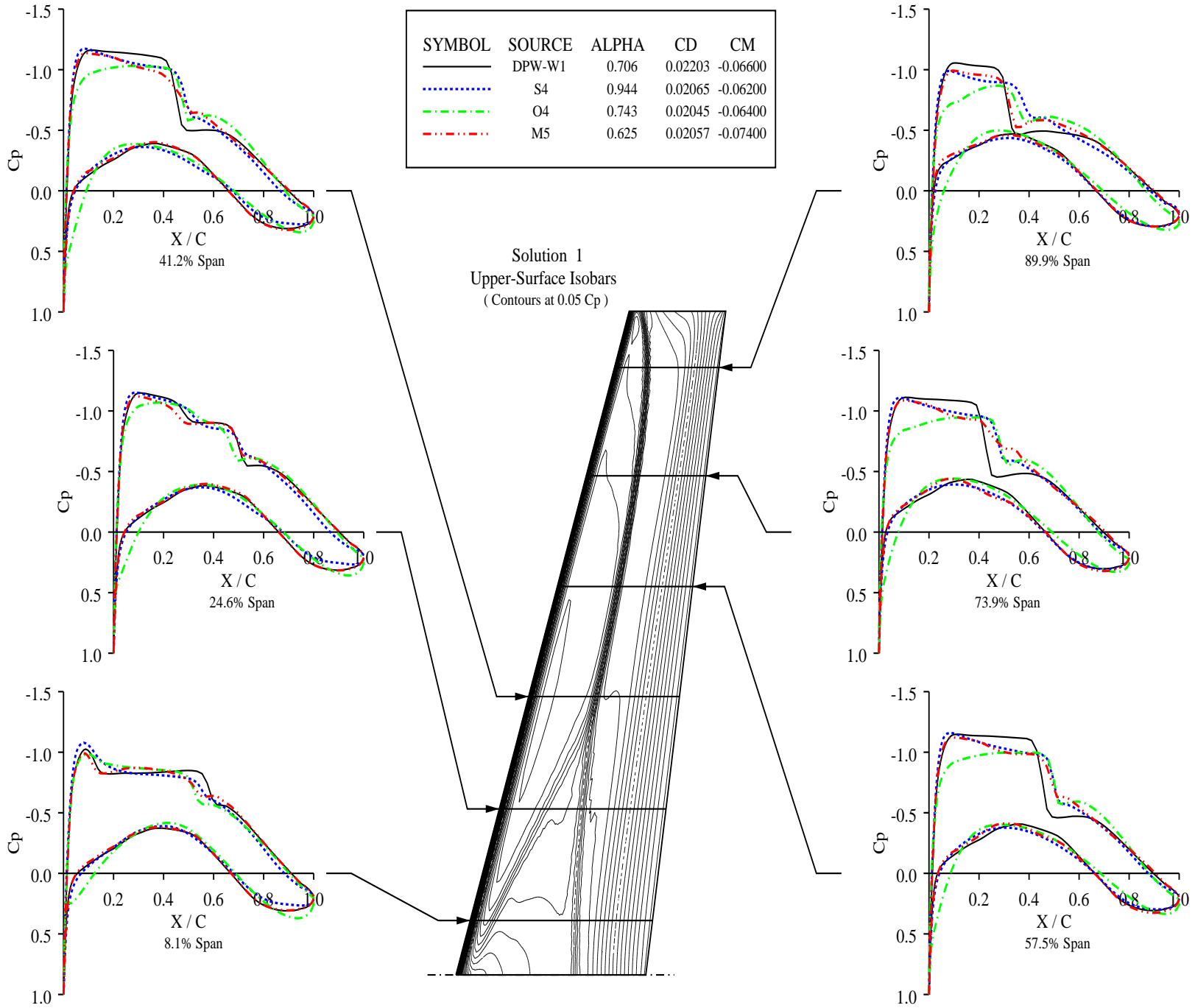


Figure 38. Comparison of chordwise pressure distributions at $M = 0.76$; $C_L = 0.5$. One-point optimization cases, OVERFLOW computations.

COMPARISON OF CHORDWISE PRESSURE DISTRIBUTIONS SINGLE-POINT OPTIMIZATIONS OF DPW-W1 WING OVERFLOW , MACH = 0.780 , CL = 0.500 , REN = 5M

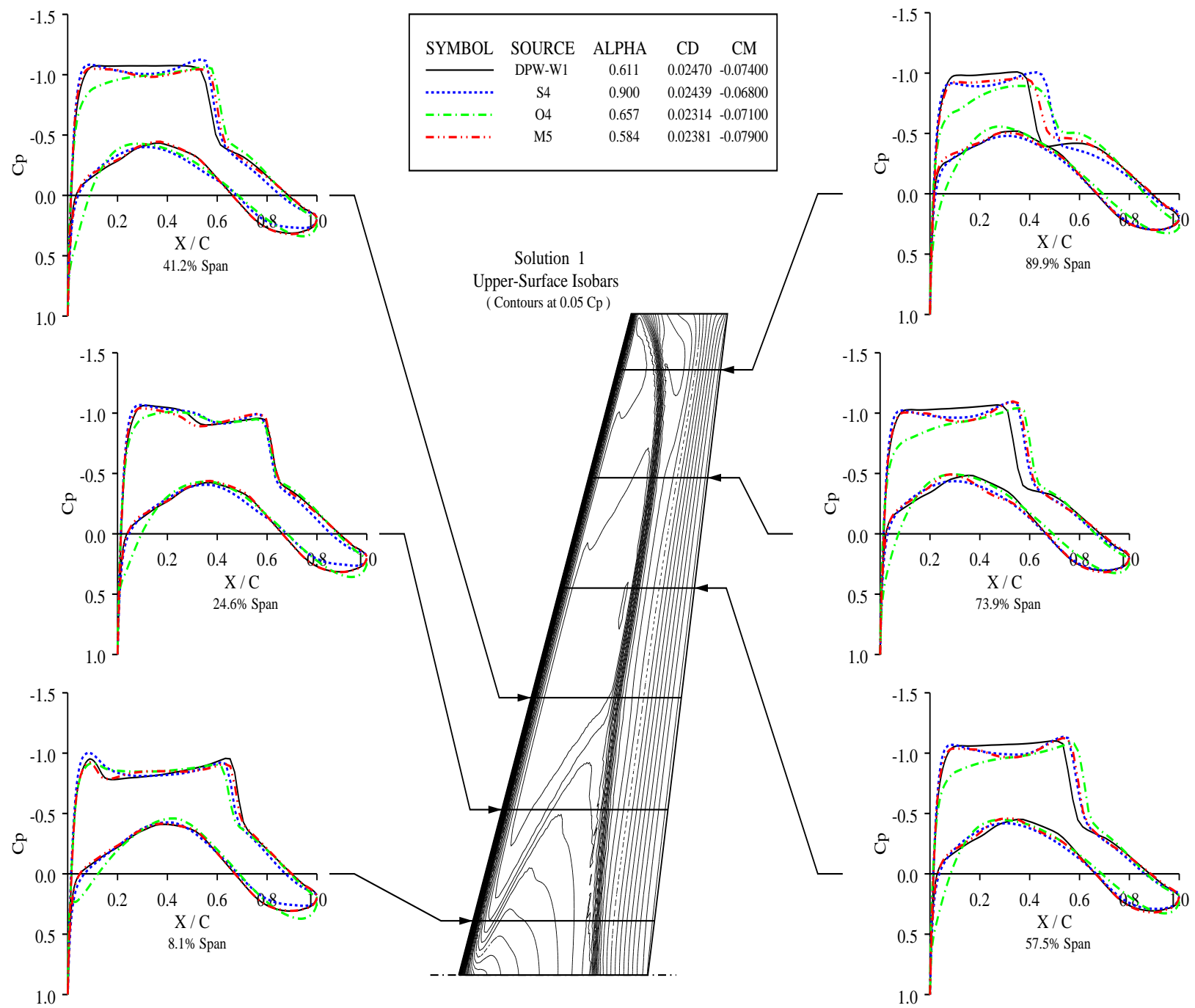


Figure 39. Comparison of chordwise pressure distributions at $M = 0.78$, $C_L = 0.5$. One-point optimization cases, OVERFLOW computations.

COMPARISON OF CHORDWISE PRESSURE DISTRIBUTIONS
 MULTI-POINT OPTIMIZATIONS OF DPW-W1 WING
 OVERFLOW , MACH = 0.760 , CL = 0.500 , REN = 5M

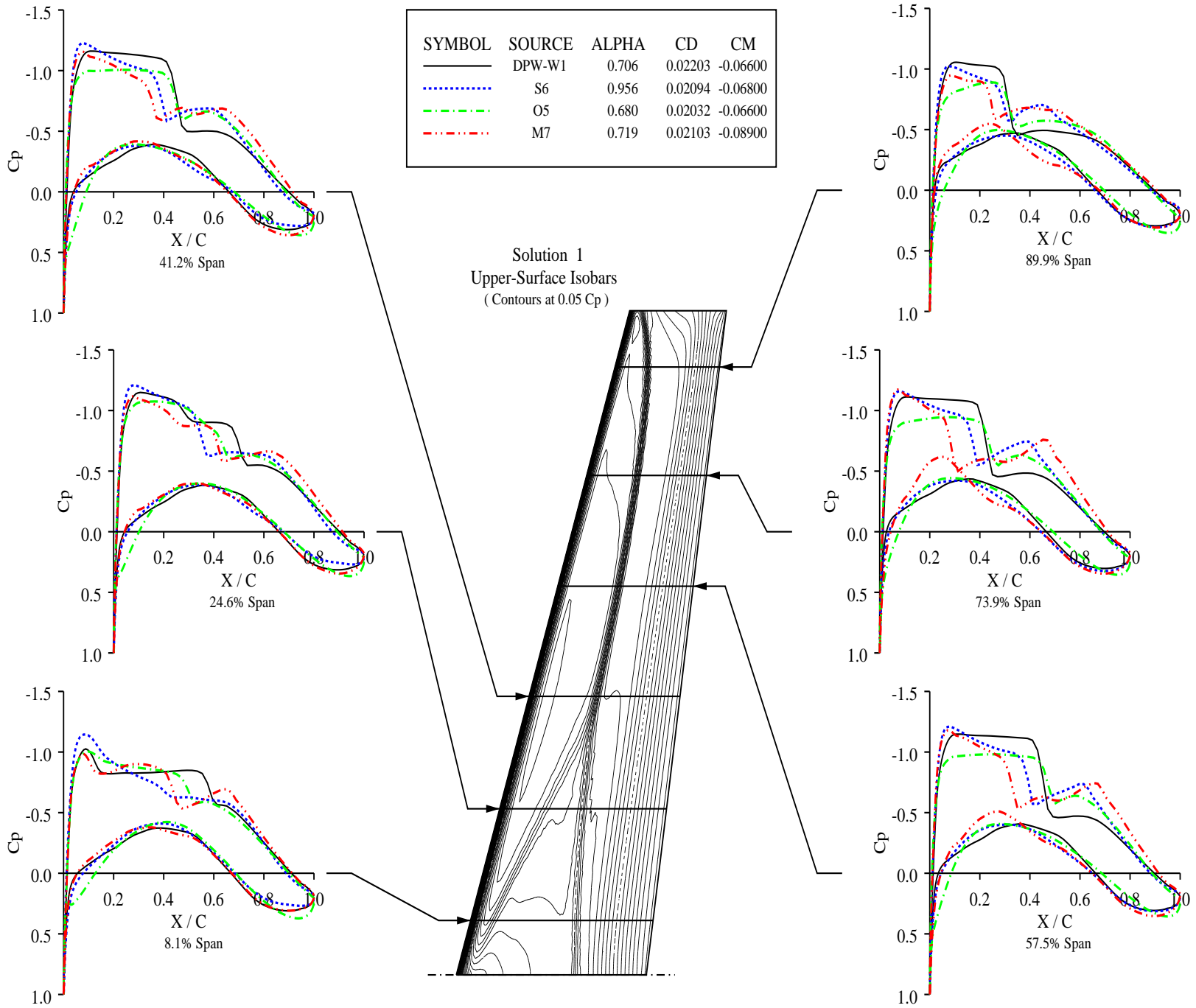


Figure 40. Comparison of chordwise pressure distributions at $M = 0.76$; $C_L = 0.5$.
 Multipoint optimization cases. OVERFLOW computations.

COMPARISON OF CHORDWISE PRESSURE DISTRIBUTIONS MULTI-POINT OPTIMIZATIONS OF DPW-W1 WING OVERFLOW , MACH = 0.780 , CL = 0.500 , REN = 5M

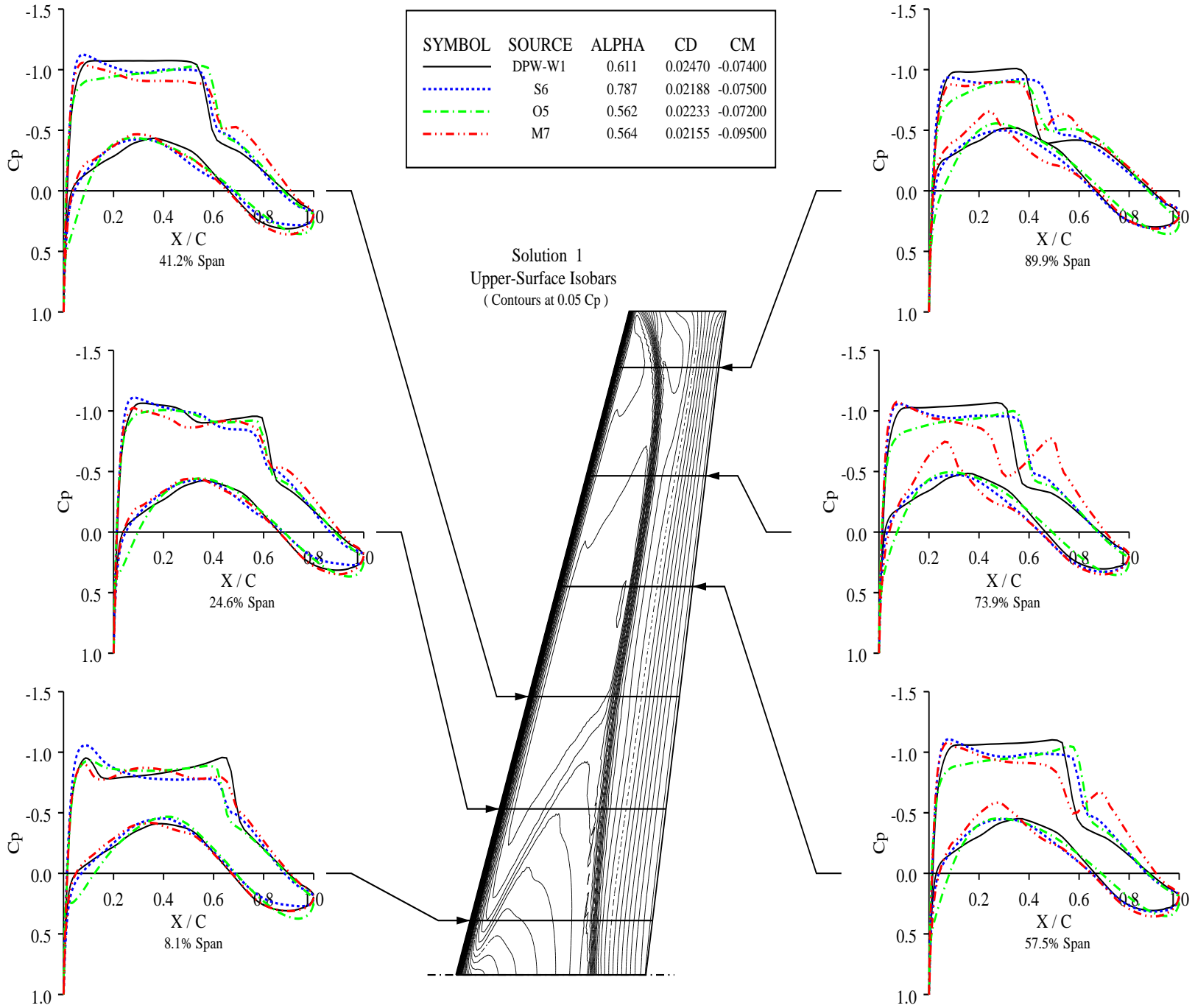


Figure 41. Comparison of chordwise pressure distributions at $M = 0.78$, $C_L = 0.5$. Multipoint optimization cases. OVERFLOW computations.

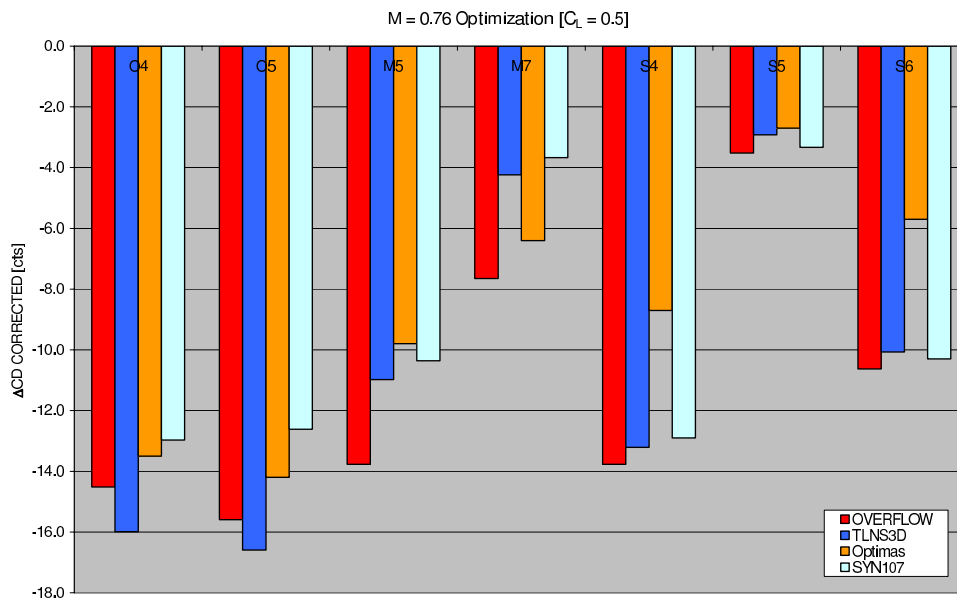


Figure 42. Corrected drag reduction values for the different optimal geometries at $M = 0.76$, $C_L = 0.5$.

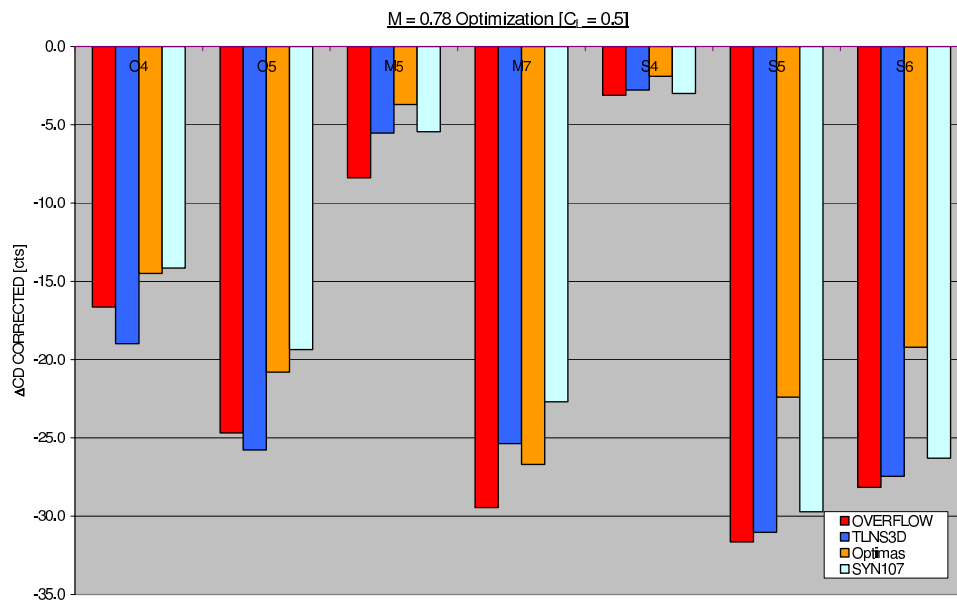


Figure 43. Corrected drag reduction values for the different optimal geometries at $M = 0.78$, $C_L = 0.5$.

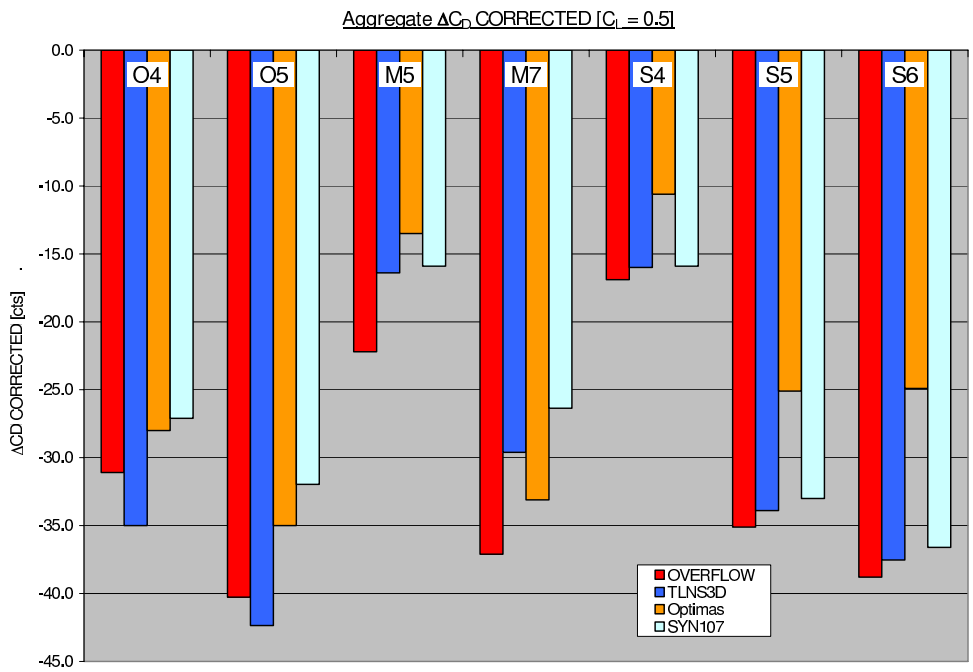


Figure 44. Corrected aggregate drag reduction values for the different optimal geometries.